Extragalactic sources towards the central region of the Galaxy

Subhashis Roy[1]⋆ A. Pramesh Rao[1] & Ravi Subrahmanyan[2]

[1] *National Centre for Radio Astrophysics (TIFR),*
Pune University Campus, Post Bag No.3, Ganeshkhind, Pune 411 007, India.
[2] *Australia Telescope National Facility, CSIRO, Locked bag 194, Narrabri, NSW 2390, Australia*

ABSTRACT

We have observed a sample of 64 small diameter sources towards the central $-6° < l < 6°$, $-2° < b < 2°$ of the Galaxy with the aim of studying the Faraday rotation measure near the Galactic Centre (GC) region. All the sources were observed at 6 and 3.6 cm wavelengths using the ATCA and the VLA. Fifty nine of these sources are inferred to be extragalactic. The observations presented here constitute the first systematic study of the radio polarisation properties of the background sources towards this direction and increases the number of known extragalactic radio sources in this part of the sky by almost an order of magnitude. Based on the morphology, spectral indices and lack of polarised emission, we identify four Galactic HII regions in the sample.

Key words: Galaxy: center – techniques: polarimetric – radio continuum: ISM – Galaxy: HII regions

1 INTRODUCTION

Since extragalactic sources are located outside the Galaxy, the effect of ISM on the propagation properties of electromagnetic waves from these objects can be modelled without distance ambiguities as in the cases of pulsars, and thereby allowing us to observe the integrated effect of the medium along large ($\sim$20 kpc) line of sight distance. Unfortunately, only a few extragalactic sources have been identified within the central few degrees of the Galaxy ($-6° < l < 6°$, $-5° < b < 5°$), which limits their usefulness as probes to study the Galactic Centre (GC) ISM. High obscuration at optical wavelengths and the confusion due to the high concentration of stars at infrared wavelengths have prevented identification of extragalactic sources in this region. High angular resolution studies at centimetre wavelengths (e.g., Becker et al. (1994) at 5 GHz and Zoonematkermani et al. (1990) at 1.4 GHz) have identified compact radio sources, but in the presence of a large number of Galactic sources near the Galactic Centre (GC), identifying the extragalactic sources is non-trivial, and only about half a dozen extragalactic sources in this region have been identified (Bower et al. 2001).

To study the Faraday rotation measure (RM) near the centre of the Galaxy ($-6° < l < 6°$, $-2° < b < 2°$), we have selected a sample of 64 small diameter ($< 10''$) sources (see Sect. 1.1) in the region, which we have studied with high angular resolution at 6 cm (C band) and 3.6 cm (X band) with the ATCA and the VLA. All the sources were studied for linear polarisation and the width of the frequency channels were chosen to avoid bandwidth depolarisation up to a RM of 15,000 rad m^{-2}. Though the NVSS (Condon et al.

1998) was capable of detecting polarised emission from sources, in those cases where the RM is high (> 350 rad m^{-2}) its bandwidth of 50 MHz would cause bandwidth depolarisation. Our observations, for the first time, provide reliable measurements of the polarisation properties of the sources in the region. These observations have almost an order of magnitude higher sensitivity (in Stokes I) and up to 3 times higher resolution as compared to the previous VLA Galactic plane survey (GPS), and this high sensitivity together with higher resolution has helped to identify the Galactic sources in the initial sample.

In this paper, we provide information on the morphology, polarisation fraction, spectral indices and rotation measure of these sources, and in a companion paper (henceforth Paper II) draw inferences about the magnetic field in the GC region.

1.1 Sample selection

We surveyed the literature and formed a sample of possible extragalactic radio sources in the central $-6°< l <6°$, $-2°< b <2°$ of the Galaxy. These sources were selected on the basis of their small scale structure ($\leqslant 10''$) and non-thermal spectra ($\alpha \leqslant -0.4$, $S(\nu) \propto \nu^{\alpha}$). For the sources to have detectable linear polarisation and so be useful for the RM study, an estimate of the polarisation fraction of the sources are required. However, in the absence of any reliable information on their polarisation fraction in the literature, we assumed the unresolved sources to be polarised at the mean polarisation fraction of extragalactic small diameter sources of 2.5% (Saikia & Salter 1988). Sources with measured flux density greater than 10 mJy at 5 GHz were selected. The source catalogues used for this selection were VLA images of the GC region at 327 MHz (LaRosa et al. 2000), the VLA survey of the Galactic plane (GPS)

⋆ E-mail: roy@ncra.tifr.res.in

at 1.4 GHz (Zoonematkermani et al. 1990), (Helfand et al. 1992) and at 5 GHz (Becker et al. 1994). Sources observed by Lazio & Cordes (1998) and the 365 MHz Texas survey (Douglas et al. 1996) were also used for this purpose. In those cases where no flux density estimates were available at 5 GHz, the flux densities at this frequency was estimated by extrapolating the 1.4 GHz flux densities using spectral indices measured between 327 MHz and 1.4 GHz. A total of 64 sources were found that satisfied all of the above criteria.

2   OBSERVATIONS AND DATA REDUCTION

Details of array configurations, frequencies used and the date of radio observations are in Table 1. The ATCA observations were made using a 6 km array configuration. Twelve sources, G357.435−0.519, G357.865−0.996, G358.002−0.636, G358.982+0.580, G359.388+0.460, G359.568+1.146, G359.844−1.843, G359.911−1.813, G0.537+0.263, G1.028−1.110, G1.035+1.559, G2.143+1.772 were observed on 06 Feb 2000 during the pilot run of the project. We observed 24 more sources G353.462−0.691, G354.719−1.117, G354.740+0.138, G356.000+0.023, G356.161+1.635, G356.567+0.869, G356.719−1.220, G358.591+0.046, G358.917+0.072, G359.546+0.988, G359.993+1.591, G0.313+1.645, G0.846+1.173, G1.505−1.231, G1.954−1.702, G2.423-1.660, G4.005+1.403, G4.188−1.680, G4.256−0.726, G4.898+1.292, G5.260−0.754, G5.358+0.899, G5.511−1.515 and G6.183−1.480 on 30th September and 02nd, 06th and 08th October, 2000. To unwrap possible $n\pi$ wrap in polarisation angles measured between two frequencies, 4 more polarised sources from the pilot run G357.865−0.996, G359.388+0.460, G0.537+0.263, G1.028−1.110 were re-observed on 06th or 08th Oct 2000. For the same reason, 4 sources from the pilot run G359.388+0.460, G359.911−1.813, G0.537+0.263, G2.143+1.772 along with G359.993+1.591 were re-observed on 12th April 2002. All these observations were made using the multi-channel continuum observing mode, and the data were acquired in 16 independent frequency channels covering 128-MHz bands centred at the observing frequencies. Each target source was typically observed for a total of 40–50 minutes. Since we used an E-W array configuration, multiple-snapshot mode was used to get a satisfactory *uv*-coverage and each source was observed ≈10 times equally spaced in hour-angle. The sources 1741−312 and 1748−253 were used to calibrate the antenna based amplitudes and phases (secondary calibrators), and their flux densities were measured based on the observation of the primary flux density calibrator PKS B1934−638. This source (polarisation fraction ⩽ 0.2%) was also used to determine antenna based polarisation leakages. The calibration and editing of the ATCA data was performed using MIRIAD. Calibrated data was converted into Stokes I, Q, U, V, and further analysis were carried out using AIPS. Maps made at different frequencies for a particular source were convolved to the same resolution. The Polarisation angle (φ) being given by φ=0.5 $\tan^{-1}(U/Q)$ (where, signs of Q and U are considered separately to unambiguously determine the value of φ), we divided the Stokes U image by the Q image and measured the polarisation angle and its error (AIPS task COMB). Finally, the polarisation angle images at different frequency bands were fitted to the equation,

$$\phi = RM.\lambda^2 + \phi_0 + n\pi \qquad (1)$$

using the AIPS task RM. In this equation, n is an integer, λ is the wavelength, and ϕ_0 denotes the intrinsic polarisation angle (i.e., when the observing frequency tends to infinity). If the rms residuals exceed four times the expected rms noise, the fitted values were rejected.

Since there were 16 frequency channels per 128 MHz band of the ATCA data, we tried to measure the RM from the ATCA observations in two ways by using the AIPS task RM. (i) Since AIPS task RM cannot fit more than four frequency channels to measure RM, in order to maximise signal to noise ratio as well as to check for high RM in the data, we divided the central 12 frequency channels of 4.8 and 5.9 GHz band into 3 equal parts. Polarisation angles were measured from first and third part of each of these bands, and these were used as input to the AIPS task RM. This allowed us to measure RM as high as 30,000 rad m^{-2}. (ii) If the RM measured by the previous method is not very high (i.e., ⩽ 2000 rad m^{-2}, and was the case for all except one source), data from each of the 4.8, 5.3, 5.9 and 8.5 GHz band were averaged and polarisation angle measured from each of these bands. These polarisation angle images and their error maps were used as the input to the AIPS task RM.

We used the VLA in its BnA configuration to observe the relatively weak sources in the sample. The default continuum mode, which provides a single frequency channel of bandwidth 50 MHz in each IF band, was used. Observations were centred at frequencies 4.63, 4.88, 8.33 and 8.68 GHz. 27 new sources, G353.410−0.360, G354.815+0.775, G355.424−0.809, G355.739+0.131, G356.905+0.082, G358.149−1.675, G358.156+0.028, G358.643−0.034, G358.605+1.440, G358.930−1.197, G359.392+1.272, G359.2−0.8 (Mouse), G359.604+0.306, G359.717−0.036, G359.710−0.904, G359.871+0.179, G0.404+1.061, G1.826+1.070, G2.922+1.028, G3.347−0.327, G3.748−1.221, G3.928+0.253, G4.005+0, G4.619+0.288, G4.752+0.255, G5.791+0.794 and G5.852+1.041 were observed on 11th and 13th February 2001 in two different bands. Moreover, the source G353.462−0.691 from ATCA observations was found to be almost unpolarised in the 6 cm band, and was re-observed on 11th February with the VLA. To unwrap possible $n\pi$ wrap in polarisation angles measured between two frequencies, 5 more sources from the ATCA pilot run, G358.002−0.636, G1.035+1.559, G359.844−1.843, G359.911−1.813 and G2.143+1.772 were re-observed on the 2nd day (13th Feb, 2001) of the VLA observations. From these sources, we re-observed G359.604+0.306 and G359.717−0.036 with the ATCA on 12th April 2002 to uniquely determine their RM.

The secondary calibrators used for the observation were the same as in the ATCA observations. Polarisation calibration was performed using the unpolarised source 3C84. 3C286 was used as the primary flux density calibrator and to estimate the instrumental phase difference between the two circularly polarised (RR and LL) antenna signals. Each source was observed for typically 5 minutes at 2 different hour angles. All the data were calibrated and processed using the AIPS package.

The source G356.905+0.082 has a compact core, which is weakly polarised, and an extended highly polarised halo. Due to zero spacing problem, the 8.5 GHz image of the halo could have missing flux density problems. Since the polarised intensity per beam of the core is similar to the contribution by the halo, which has small scale structures in polarised image and is not properly sampled at 8.5 GHz, we could not reliably estimate the RM from the core or the halo. Therefore, we have not provided its RM in Table 6.

Table 1. Journal of observations

Epoch	Telescope	Array config-uration	Obs. time (hours)	Frequency (GHz)	No. of sources observed
06 Feb 2000	ATCA	6A	10	4.80 & 5.95	12
30 Sept 2000	ATCA	6B	12	4.80 & 5.95	12
02 Oct 2000	ATCA	6B	12	4.80 & 5.95	12
06 Oct 2000	ATCA	6B	12	5.31 & 8.51	14
08 Oct 2000	ATCA	6B	12	5.31 & 8.51	13
11 Feb 2001	VLA	BnA	06	4.63 & 4.88	28
13 Feb 2001	VLA	BnA	06	8.33 & 8.68	32
12 Apr 2002	ATCA	6B	11	5.06 & 5.70	08

3 RESULTS

Based on the ATCA data, 24 sources were found to have at least one polarised component. Images of these sources are shown in Fig. 3. The FWHM sizes of the beams in the ATCA images are $\approx 6'' \times 2''$, and the typical RMS noise is 0.23 mJy/beam in Stokes I and about 0.15 mJy/beam in Stokes Q and U. These images show 7 of the 24 sources to have a single unresolved component and the remainder are either partially resolved or have multiple components.

Of the sources observed using the VLA, 21 have at least one polarised component. Images of these sources along with 2 po-larised phase calibrators are shown in Fig. 4. The FWHM sizes of the beams in the VLA images are $\sim 2'' \times 1.5''$ and the RMS noise is typically 75 μJy/beam. In these images, four sources appear as single unresolved components. Since $1741-312$ and $1748-253$ have been observed by both ATCA and the VLA, but $1741-312$ has a faint emission around the compact source as seen in higher resolution VLA maps, we have presented its properties in Stokes I from the VLA data.

Stokes I images of the sources in the sample that were not detected to have polarised emission are shown in Fig. 5 and Fig. 6 respectively.

The properties of the 24 polarised sources observed with ATCA are presented in Table 2 and 21 sources observed with VLA are in Table 3. In these tables, the following conventions are used. Column 1: the source name using Galactic co-ordinates ($l \pm b$). Column 2: the component designation; 'N' denotes Northern, 'S' denotes Southern, 'E' denotes Eastern and 'W' denotes Western, 'C' denotes central, 'EX' denotes highly extended and 'R' denotes ring type. Columns 3 and 4: Right ascension (RA) and Declina-tion (DEC) of the radio intensity peaks of the components in J2000 co-ordinates. Column 5: the deconvolved size of the components with their major and minor axes in arc-seconds and the position angle (PA) in degrees (formatted as major axis $\times$ minor axis, PA). A few sources that are observed to have multiple resolved com-ponents in the 8.5 GHz images are, however, not well resolved in the 4.8 GHz images. For these sources, we have measured the size parameters of the components from the 8.5 GHz images and we put a '*' symbol beside these measured parameters. Columns 6 and 7: the corresponding peak and total flux density of the com-ponents at 4.8 GHz in units of mJy beam^{-1} and mJy respectively. Column 8: total flux density of the component at 4.8 GHz as mea-sured by the VLA GPS survey. Column 9: percentage polarisation of the components. Column 10: spectral indices of the components measured between 8.5 and 4.8 GHz. A few of the sources are ex-tended over several synthesised beam-widths and for these sources we have convolved the 8.5 GHz images to the resolution at 4.8 GHz and then made spectral index images. The spectral indices of the in-dividual components are measured from these images, we put an 's' beside the spectral index for these extended sources. Columns 11 and 12: spectral indices between 4.8 and 1.4 and between 1.4 and 0.3 GHz respectively. Column 13: the source classification; 'EG' denotes an extragalactic source (based on the morphology), and G denotes a Galactic source. Several sources show the morphology typical of FR$-$I or FR$-$II sources and this is noted along with the extragalactic classification. Sources which appear unresolved (de-convolved source size $<<$ beam size) are denoted by U, slightly resolved (deconvolved source size $\lesssim$ beam size) by SR, double by D and T denotes a triple source consisting of a pair of lobes and a core. C+E denotes a flat spectrum core with extended emission either in the form of a lobe or jet. If there are several objects in the field which appear to be unrelated, we label the object as M.

For computing spectral indices in Table 2 and 3, the 1.4 GHz flux densities of the sources have been taken from the VLA GPS and the NRAO VLA Sky Survey (NVSS) (Condon et al. 1998). If the measured flux density of a component in the GPS differs from that in the NVSS by more than 20%, we have put a '†' mark beside the computed spectral indices (column 11). We have visu-ally examined the NVSS images of these sources and if we find that the source is not in a confused region of the image we have used the flux density from NVSS to compute the spectral index; in such cases, we put '(N)' beside the measured spectral index. For the source G359.871+0.171, the 1.4 GHz flux density has been as-sumed to be the same as that measured by Lazio et al. (1999) at 1.5 GHz and we put '(L)' beside its measured spectral index be-tween 4.8 and 1.4 GHz. For a few sources in the list, the 1.4 GHz flux density in unknown. In these cases, we put a '**' in column 11 and enter the spectral index between 4.8 and 0.3 GHz in column 12 with '(0.3/4.8)' written below. The P-band flux densities of the sources have been taken from the Texas survey at 365 MHz (Dou-glas et al. 1996). However, the Texas survey is known to have large uncertainty in flux densities for sources near the Galactic plane and which is more near the complex GC region. Therefore, if any source is detected in the GC image at 330 MHz (LaRosa et al. 2000), we have used their flux density to compute the spectral index (column 12 in Table 2, 3 and column 11 in Table 4, 5) and put 'GC' in paren-thesis beside the spectral index measured. For 5 sources the flux densities at 330 MHz have been taken from Roy & Rao (2002), and we put '(GM)' beside the spectral index in column 12. We have also taken the flux densities of 3 sources at 330 MHz from S. Bhatnagar (private communication) and put '(GM1)' in column 12. Many of the sources resolved at frequencies of 1.4 GHz and above appear unresolved in the low frequency Texas survey. For these sources, we only compare their integrated flux densities between 1.4 and 0.3 GHz, and put '(i)' beside the measured spectral index in col-umn 12.

In Table 4 & 5 we present the properties of the sources which are not detected in polarised emission. These tables are similar to Table 2 & 3, except that we have omitted the column representing percentage polarisation (column 9 in Table 2 & 3). For the four Galactic HII regions we have identified, we write 'G$-$HII' in col-umn 12 of this Table.

The measured RM towards 44 sources (65 components) and 2 secondary calibrators are given in Table 6, which is arranged as follows:
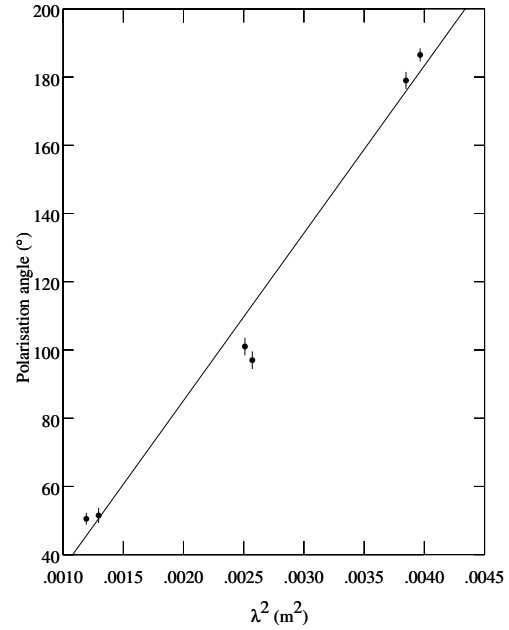
Column 1: the source name in Galactic co-ordinates (G$l\pm$b). Col-umn 2 & 3: RA (J2000) and DEC (J2000) of the source compo-nents. The co-ordinates of these components are based on the peak in the polarised intensity (if the peak in the polarised intensity do not coincide with the peak in total intensity, the component position

will be slightly different than what is given in Table 2 & 3 based on the peak in total intensity). Column 4 & 5: the measured RM (in rad m^{-2}) and the error in these measurements at the position of the peak in the polarised emission. Depolarisation fraction is defined as the ratio of the polarisation fraction of any component between lower to that at higher frequency, and in column 6 we provide the depolarisation fraction (D) of the source components between 4.8 and 8.5 GHz. Column 7: Percentage error in the depolarisation fraction (Δ(D) in %). Assuming that the emission mechanism is synchrotron, the orientation of the electric field in the radiation has been used to infer the orientation of the magnetic field in the plasma and we provide the direction of this magnetic field (θ) and the error in this measurement ($\Delta\theta$) in columns 8 & 9 respectively. Column 10: Reduced Chi-square (χ^2) of the fit of Equation 1 to the measured polarisation angles. We show an example of bad fit (χ^2=17) in Fig. 1, and one example of good fit (χ^2=0.2) in Fig. 2. Column 11: Measured polarisation angles at different frequencies. The observed frequencies (in MHz) and the measured polarisation angles (in degrees) are tabulated in pairs, and each frequency, polarisation angle pair are separated by commas.

The source G359.2−0.8 (Mouse) is a known Galactic non-thermal source. Since this source is known to be within 5 kpc from the Sun (Uchida et al. 1992), the RM towards this object is expected to be quite small. To check if observations confirm its low RM, we observed this source. From Table 6, its RM is indeed measured to be very small (−5 ±18 rad m^{-2}). However, our samples are selected to measure the RM introduced by the GC region, but this source only samples the local ISM, and its RM is not used in any further analysis.

3.1 Accuracy of the spectral index measurements

The errors in the derived spectral indices depend on the accuracies of the flux densities at different frequencies. One of the drawbacks of a Fourier synthesis array is that if a source is resolved on the shortest interferometer baseline, its flux density will most likely be underestimated in the image. In the GC region, where the sky density of sources is high and emission at various size scales may co-exist, confusion could be a significant source of errors in imaging and hence in flux density estimates. Because our radio observations are performed at relatively high frequencies, the contribution from extended Galactic synchrotron background is negligible. Additionally, most of the sources in our sample have small angular sizes and, therefore, the problem of missing flux density should be minimal. The ATCA and VLA observations were both made using a single array at both the frequencies. Since problem of any missing flux density increases with increase in observing frequency, this might result in an underestimation of the source spectral index. We have detected extended emission of up to ∼10′ scale in our 4.8 GHz images of G353.410−0.360, G355.424−0.809, G355.739+0.131, G356.905+0.082, G358.149−1.675, G358.643−0.034, G359.2−0.8 (Mouse), G359.717−0.036, G0.313+1.645 and G5.791+0.794. To examine for any missing flux density at 8.5 GHz, we first restricted the Fourier Transform of the CLEAN components of the 4.8 GHz images to the *uv*-range of the 8.5 GHz visibilities. A comparison of the corresponding images with the original 4.8 GHz images (without the restriction in visibility coverage) shows that except for G353.410−0.360, G355.739+0.131, G356.905+0.082, G358.643−0.034, G358.149−1.675, G359.2−0.8 (Mouse) and G359.717−0.036, the missing flux density is less than 10% of the total flux density, and the corrsesponding error in their spectral

Figure 1. An example of bad fit of Equation 1 to the measured polarisation angles vs. square of wavelength plot (reduced χ^2=17). The polarisation angles are measured towards the source G358.002−0.636.
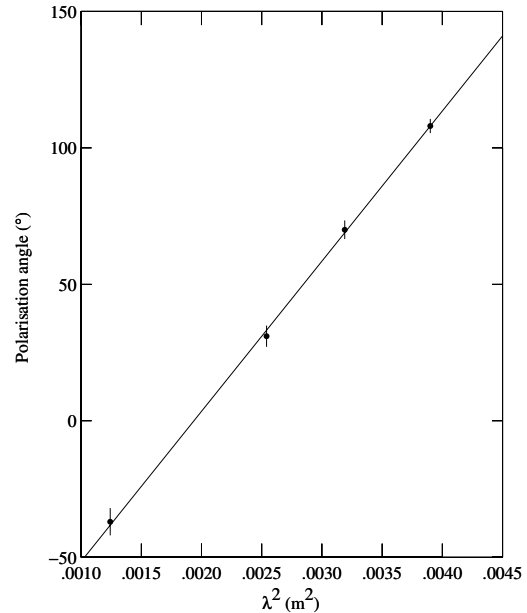
Figure 2. An example of good fit of Equation 1 to the measured polarisation angles vs. square of wavelength plot (reduced χ^2=0.2). The polarisation angles are measured towards the source G356.567+0.869.

indices between 8.5 and 4.8 GHz is less than 0.25. Among the above 7 sources, 4 have been identified as HII regions. The spectral indices between 8.5 and 4.8 GHz of the 2 remaining extragalactic sources G356.905+0.082 and G358.149−1.675 and the Galactic non-thermal source G359.2−0.8 (Mouse) (Table 3) have been measured only for the compact components (e.g., core and hot spots). For other sources, the error in the measured flux densities are expected to be about 5%, and the corresponding error in their spectral indices between 8.5 and 4.8 GHz is about 0.1.

Owing to extended emission and enhanced source confusion near the GC, images made from radio interferometers and with sparse spatial frequency coverage suffer from systematic errors. To estimate the errors in the source flux densities in the GPS and Texas survey, we compared the 1.4 GHz flux densities of our sample sources as measured by the GPS and the NVSS and found that the differences in flux density measurements were about 20 per cent. 20% differences in flux density contributes an error of about 0.15 in the measured spectral index between 4.8 and 1.4 GHz. We also compared the flux densities of the 12 sources which are detected in both the Texas survey and in the 330 MHz VLA GC image (LaRosa et al. 2000) and noticed that the difference is almost a factor of two for six of these sources. The errors in the flux density measurents from the GC image are expected to be relatively smaller and, therefore, if the 0.3 GHz flux density of a source is taken from the Texas survey, an error ∼0.5 can occur in its spectral index measurement between 1.4 and 0.3 GHz. We note that other than the missing flux density problem, there are several other systematic errors which could lead to erroneous measurement of spectral indices. One of these errors is source variability, which we discuss below.

3.2   Effect of source variability

Estimation of source spectral indices and the RM requires multi-frequency observations. Most of our multifrequency observations were separated by a time period, which varies from a few days to an year or two. Any source variability in these timescale will affect the measured spectral indices and possibly the measured RM. However, we note that the variability of the extragalactic sources at frequencies higher than a few GHz is often intrinsic in nature (Wagner & Witzel 1995) and in some cases caused by interstellar scintillation (ISS) (Lovell et al. 2003). The typical variability timescale for intrinsic variability is from a few hours to years (Wagner & Witzel 1995), and from hours to months in the case of ISS (Lovell et al. 2003). However, only the core dominated objects with flat spectrum ($\alpha > -0.5$) can show significant variability in timescale of days or less (Wagner & Witzel 1995). Among the sources observed, only G356.905+0.082, G357.865−0.996, G358.002−0.636, G0.537+0.263, G3.928+0.253 falls into this category. Among them, the multifrequency observations of G356.905+0.082 and G3.928+0.253 were separated by only 2 days, and the probability of significant variability at this timescale is believed to be low. As described below, G357.865−0.996 is variable, G0.537+0.263 does not appear to be variable, and we do not have data to check for variability of G358.002−0.636. We note that variability in timescale of few hours could not be identified for any of our sources.

We identify 12 sources from Sect. 2, G357.865−0.996, G358.002−0.636, G359.388+0.460, G359.604+0.306, G359.717−0.036, G359.844−1.843, G359.911−1.813, G359.993+1.591, G0.537+0.263, G1.028−1.110, G1.035+1.559, G2.143+1.772, towards which our observations were separated upto 2 years, and their measured properties could suffer substan-

tially from variability. Among these sources G1.028−1.110, G1.035+1.559, G359.604+0.306, G359.717−0.036 and G359.993+1.591 are extended (more than few arc seconds in angular size). Consequently, their variability timescale will be many years, and they are not considered to be variable in this paper. Among the rest of the sources, G357.865−0.996, G359.388+0.460, G0.537+0.263, G359.911−1.813, G2.143+1.772 were observed with ATCA on days, where certain frequency band was common to both the epochs. On comparing the flux densities of these sources in the same band (with appropriate correction of flux densities from their measured spectral indices due to change of frequency), from both the observing days, it was found that only the flux density of the source G357.865−0.996 has changed by more than 10%. Unfortunately, such a method could not be applied for the remaining 2 sources G358.002−0.636 and G359.844−1.843. Since, G359.844−1.843 is a steep spectrum source (Table 2), the emission from it is likely to be originated from extended region (e.g., from jets), and the variability timescale is large. However, G358.002−0.636 is a rather flat spectrum source (core dominated), and could be variable. We note that the fit of Equation 1 to its polarisation angles is bad (Reduced χ^2=17, Table 6), and one possible reason for this is source variability. Consequently, the measured RM of G357.865−0.996 and G358.002−0.636 is excluded from the sample used to derive statistical estimates of the RM introduced by the GC region. We do not consider the effect of variability on the spectral indices of sources estimated from other catalogues (i.e., other than $\alpha_{8.5/4.8}$).

3.3   Contribution of the intrinsic Faraday rotation to the measured RM

When the polarised emission from the source reaches the observer, rotation of the polarisation angle could occur (i) within the source, (ii) in the Inter Galactic Medium (IGM) or (iii) in the ISM of the Galaxy. Compared to the ISM of our Galaxy, the electron density of the IGM is very small, and consequently the Faraday rotation introduced by the IGM is negligible. However, if the synchrotron electrons are mixed with thermal electrons at the source, or, if there is an intervening galaxy, the ISM of which introduces RM, or if there is cluster of galaxies along the line of sight, there can be Faraday rotation introduced outside our Galaxy. As discussed by Gardner & Whiteoak (1966); Kronberg et al. (1972); Vallee (1980), the polarisation angle could deviate from the λ^2 law due to the following three mechanisms.
(i) If the synchrotron optical depth becomes significant at some frequency, the polarisation direction makes a transition from parallel to perpendicular to the projected magnetic field. (ii) If there are multiple unresolved emission components with differing spectral indices and polarisation characteristics, it can cause complex wavelength dependent variations in polarisation angle. (iii) If there are significant gradients in Faraday rotation across or through the emission region of the source, then also polarisation angle can have complex dependence on the observing wavelength. The polarisation angles of the source G358.002−0.636 deviates significantly from the λ^2 law, and other than source variability (Sect. 3.2), it could have been caused by one of the above processes.

In the case of Faraday rotation outside the Galaxy, the Faraday screen is likely to be located several orders of magnitude farther away than the GC ISM. As a result, emission from different parts of the source is viewed within one synthesised beam, the linear scale of which is much larger than what is sampled in our ISM. At such length scales (∼1 kpc), the magnetic field within the in-

tervening Faraday screen is likely to be uncorrelated. As a result, there is differential Faraday rotation within the beam, which gives rise to source depolarisation. From the data, the RM towards the source G358.917+0.072 is found to be the highest with a measured value of 4768 rad m^{-2}, and it shows a high depolarisation fraction (0.3 between 4.8 and 8.5 GHz), which is likely to be caused by differential Faraday rotation (Kronberg et al. 1972).

Following the arguments given above, if the reduced χ^2 of the fit is greater that 4.6, the probability of occurrence of which is less than 1% (Bevington 1969) or any of the source component shows a depolarisation fraction of less than 0.6 (Table 6) between 4.8 and 8.5 GHz, we suspect that there is significant RM introduced outside the Galaxy and the RM towards those components have not been used any further in this or in deriving the properties of the Faraday screen in Paper II. We note that the intrinsic RM of most of the extragalactic sources are quite small ~ 10 rad m^{-2} (Simard-Normandin & Kronberg 1980) and the RMs measured from our sample is quite high (~ 1000 rad m^{-2}), and consequently the RM introduced outside the Galaxy should have little effect on the RMs of most of the sources in our sample.

Table 2: Measured parameters of the polarised sources from the ATCA data

Source	Cmp	RA (J2000)	DEC (J2000)	$S_{maj} \times S_{min}$, PA	S_p	S_t mJy	S_5 mJy	% Poln.	$\alpha_{8.5/4.8}$	$\alpha_{4.8/1.4}$	$\alpha_{1.4/0.3}$	Notes
354.740+0.138	N	17 31 56.99	−33 18 34.1	0.8×0.0, 146	61	67	52.6	2.6	−1.2	−1.0†	−0.8 (i)	EG−SR
	S	17 31 57.00	−33 18 41.6	4.3×1.6, 0	14	13		8	−1.1			
356.000+0.023	E	17 35 39.74	−32 18 54.2	2.3×1.2, 103*	30	42	34.7	7	−0.9	−0.8	−1.1 (GM)	EG−T
	C	17 35 40.15	−32 18 57.0	0.9×0.0, 24*	29	34		9	−0.6	−0.5		
	W	17 35 40.40	−32 18 59.0	1.3×1.1, 107*	36	38	79.2	6	−1.0	−0.6(i)		
356.161+1.635	E	17 29 42.63	−31 18 02.1	3.1×1.0, 81	21	38		5.6	−1.1	−0.7	−0.9 (i)	EG−D
	W	17 29 43.80	−31 18 05.6	2.4×0.7, 101	44	69		11	−1.0	−0.8		
356.567+0.869	N	17 33 44.85	−31 22 33.6	6.1×4.4, 119	11	31			−1.5	−0.55†	−0.9 (i)	EG−D
	S	17 33 45.82	−31 22 51.2	3.4×1.3, 140	21	46		14	−1.6	−0.65		
356.719−1.220	E	17 42 27.41	−32 22 08.3	3.4×2.1, 141	19	30		11	−1.0	−0.8	−0.9 (i)	EG−D
	W	17 42 27.96	−32 22 15.3	2.0×1.8, 102	24	35		7	−1.0	−0.6		
358.002−0.636	C	17 43 17.87	−30 58 18.7	0.4×0.0, 165	277	283		1	−0.4	−0.26	−0.3	EG−U
358.917+0.072	C	17 42 44.00	−29 49 16.0	0.3×0.0, 2	99	101	74	1.5	−1.4	−1.05	−1.2 (GC)	EG−U
359.388+0.460	C	17 42 21.47	−29 13 00.9	0.5×0.0, 178	39	41		3	−0.9	−0.65†	−0.4 (GC)	EG−U
359.844−1.843	C	17 52 30.91	−30 01 06.6	1.4×1.0, 74	154	181		1.6	−0.6	−0.2	−0.9 (GC)	EG−SR
359.911−1.813	C	17 52 33.1	−29 56 44.8	0.6×0.0, 01	132	149		4	−0.9	−0.2	−0.9 (GC)	EG−U
359.993+1.591	E	17 39 26.49	−28 06 18.2	1.2×0.0, 176	13	14			−1.2	−0.9	−0.5 (GC)	EG−D
	W	17 39 26.94	−28 06 12.6	1.5×0.0,46	11	12		10	−0.8	−0.66		
0.313+1.645	E	17 40 00.27	−27 48 11.6	3.4×2.1, 144*	17	32		16	−0.7	−0.6	−0.55 (GC)	EG−T
	C	17 40 00.65	−27 48 15.9	2.3×0.9, 155*	07	08			−0.1			
	W	17 40 01.08	−27 48 22.0	2.3×0.0, 131*	11	21			−1.3	−0.8		
0.537+0.263	C	17 45 52.48	−28 20 26.6	2.5×0.0, 175	71	79	121	1.6	0.64	0.44		EG−U
1.028−1.110	N	17 52 22.51	−28 37 34.1	2.4×0.9, 153	23	26		6	−1.1	−0.8	−1.0 (GC)	EG−D
	S	17 52 22.81	−28 37 42.1	1.3×0.0, 142	40	45		6	−1.1	−1.0		
1.035+1.559	N	17 42 01.90	−27 13 10.3	2.3×0.0, 17	50	67		24	−1.2	−0.73	−0.86 (GC)	EG−T
	C	17 42 03.42	−27 14 16.3	1.7×0.0, 85	02	02			0.0			
	S	17 42 05.22	−27 15 10.2	3.7×2.6, 119	02	09						

Source	Cmp	RA (J2000)	DEC (J2000)	$S_{maj} \times S_{min}$, PA	S_p	S_t mJy	S_5 mJy	% Pol.	$\alpha_{8.5/4.8}$	$\alpha_{4.8/1.4}$	$\alpha_{1.4/0.3}$	Notes
1.505−1.231	E	17 53 55.37	−28 15 53.8	1.8×0.8, 109	30	56		17	−1.7	−0.43	−1.3 (i)	EG-D
	W	17 53 59.21	−28 17 21.3	0.7×0.0, 13	23	25		12	−1.0	−0.7		
2.143+1.772	C	17 43 51.24	−26 10 59.6	0.8×0.4, 150	45	48		4.5	−1.5	−1.25	−1.1	EG-U
4.005+1.403	S	17 49 31.68	−24 46 58.5	1.7×0.0, 163	52	71		4	−0.8	−0.7	−0.8 (i)	EG-D
	N	17 49 32.30	−24 46 45.7		01	03						
4.188−1.680	S	18 01 44.34	−26 10 43.6	1.8×0.7, 25	29	44		13	−1.4	−0.5	−1.3 (i)	FR-II
	C	18 01 45.97	−26 10 17.6	1.4×0.6, 22	06	06			−0.7			
	N	18 01 47.04	−26 10 02.0	6.7×4.2, 16	04	16			<−2.0	−0.84		
4.256−0.726	E	17 58 11.76	−25 38 49.1	1.0×0.0, 165	08	09			−0.8	−0.8	−0.84 (i)	EG-D
	W	17 58 13.00	−25 38 44.7	1.7×0.5, 63	13	17		18	−1.5	−1.0		
5.260−0.754	C	18 00 31.50	−24 47 21.3	0.7×0.5, 68*; 0.6×0.4, 84*	66	89		10	−0.8	−0.8	−0.45	EG-U
5.358+0.899	E	17 54 27.34	−23 52 33.8	1.4×0.0, 8*; 1.7×0.5, 7*	24	45			−0.4	−0.85	−0.95 (i)	EG-T
	W	17 54 27.78	−23 52 36.2	0.8×0.2, 40*	31	33		6	−1.2	−0.9		
5.511−1.515	S	18 03 59.28	−24 56 45.6	5.3×1.0, 01	62	85		4	−0.8	−0.6	−1.1	EG-D
	N	18 03 59.43	−24 56 30.8		02	04				−0.8		
6.183−1.480	N	18 05 18.04	−24 20 26.7	3.6×1.6, 09	08	10		14	−0.8	−1.0†	−1.2 (i)	EG-D
	S	18 05 18.04	−24 20 45.5	3.6×0.9, 08	19	24			−1.1	−0.9		

Note: In Table 2, 3, 4 and 5 of this paper, the symbols shown below indicate the following

'*' – size of the object estimated from 8.5 GHz map

s – Spectral index estimated by dividing images made at different frequencies

G – Galactic source

EG – Extragalactic source

U – Unresolved source

SR – Slightly resolved

D – Double source

T – Tripple

C+E – Flat spectrum core with extended emission.

M – Multiple sources in the field

† – 1.4 GHz GPS flux density differs from NVSS by more than 20%

(N) – 1.4 GHz flux density taken from NVSS

(L) – Flux density taken from Lazio et al. (1999)

** – 1.4 GHz flux density unknown

Source	Cmp	RA (J2000)	DEC (J2000)	$Smaj \times S_{min}$, PA	S_p	S_t mJy	S_5 mJy	% Pol.	$\alpha_{8.5/4.8}$	$\alpha_{4.8/1.4}$	$\alpha_{1.4/0.3}$	Notes
353.462−0.691	C	17 31 55.40	−34 49 59.9	0.4×0.2, 165	98	103		0.6	−0.9	−0.9	−0.7	EG–U

(GC) – P band flux density taken from (LaRosa et al. 2000)
(GM) – P band flux density taken from Roy & Rao (2002)
(GM1) – P band flux density taken from S. Bhatnagar (private communication)
(i) – Spectral index estimated from integrated flux densities of components

Table 3: Measured parameters of the polarised sources from VLA data

Source	Cmp	RA (J2000)	DEC (J2000)	$Smaj \times S_{min}$, PA	S_p	S_t mJy	S_5 mJy	% Poln.	$\alpha_{8.5/4.8}$	$\alpha_{4.8/1.4}$	$\alpha_{1.4/0.3}$	Notes
354.815+0.775	E	17 29 36.26	−32 53 52.1	0.8×0.5, 71	6.8	8.2			−1.2	−1.0	−0.9 (i)	EG–D
	W	17 29 36.64	−32 53 51.7	0.5×0.4, 176	18.2	20.2		5	−1.4	−1.0		
355.424−0.809	N	17 37 32.54	−33 14 36.7	2.7×1.3, 57	6.5	22		20	−1.0 s	−1.0 (N)	−0.9	FR–II
	C	17 37 32.07	−33 14 50.7	1.5×1.0, 167	1.0	1.1			−1.0 s			
	S	17 37 31.40	−33 15 10.4	1.5×1.1, 176	11	24		12	−0.8 s			
356.905+0.082	C	17 37 43.79	−31 31 13.7	3.6×0.4, 179	40	43	32	3	−0.1		−0.4 (GM)(i)	FR–I
357.865−0.996 (1741−312)	C	17 44 23.58	−31 16 36.0	0.1×0.0, 22	369	370		1.4	0.2	0.4†	−0.5 (i)	C+E
358.149−1.675	E	17 47 45.32	−31 23 37.4	2.1×1.4, 124	8.9	57		25	−1.0 s	−1.0 (N)	−0.77	FR–II
	C	17 47 48.13	−31 23 15.2	0.3×0.0, 18	7.4	7.6			0.1 s			
	W	17 47 50.13	−31 23 03.9	0.7×0.4, 60	13	98		12	−0.8 s			
358.156+0.028	N	17 41 02.91	−30 29 22.1	0.5×0.5, 113	23.7	30	31	13	−0.9	−0.6	−1.0 (GC)	FR–II
	C	17 41 02.90	−30 29 27.3	0.5×0.0, 04	1.7	1.5			−0.1			
	S	17 41 02.67	−30 29 36.1	1.5×0.7, 39	3.0	4.2	5.2	21	−0.8	−0.86		
358.930−1.197	E	17 47 46.36	−30 28 17.8	1.5×0.9, 27	8.9	22		26	−0.6 s	−0.4 (i)	−1.4 (GC)	EG–D
	W	17 47 47.54	−30 28 11.7	2.6×1.3, 22	4.5	14.8			−0.7 s			
359.392+1.272	E	17 39 12.44	−28 47 02.7	2.2×1.2, 33	6.9	24.5		16	−0.6	−0.9 (N)	−0.76 (GC)	FR–II
	W	17 39 13.46	−28 46 53.7	2.8×1.5, 40	5.1	20.4		20	−0.7			
359.2−0.8 (Mouse)	C	17 47 15.78	−29 58 01.0	3.2×2.2, 20	11.3	20.2		13	0.3		−0.3 (GC)(i)	G
359.604+0.306	E	17 43 28.39	−29 06 47.6	2.8×1.0, 77	2.6	7.7	−		−1.0	**	−0.8 (GC)(i) (0.3/4.8)	FR–II
	C	17 43 28.77	−29 06 47.0	0.7×0.1, 81	2.5	2.7	3.3		−0.1			
	W	17 43 29.26	−29 06 47.1	1.4×0.9, 14	6.7	10.8	7.6	12	−1.0			

Source	Cmp	RA (J2000)	DEC (J2000)	$Smaj \times S_{min}$, PA	S_p	S_t mJy	S_5 mJy	% Pol.	$\alpha_{8.5/4.8}$	$\alpha_{4.8/1.4}$	$\alpha_{1.4/0.3}$	Notes
359.710−0.904	E	17 48 27.73	−29 39 10.3	4.0×1.9, 67	2.4	23		23	−1.4	**	−0.75 (GC)	FR-II?
	C	17 48 28.58	−29 39 10.9	0.4×0.0, 52	0.7	0.7			−1.5		(0.3/4.8)	
	W	17 48 29.39	−29 39 11.8	5.5×2.5, 90	2.3	23.6		15	−1.7			
359.871+0.179	E	17 44 36.22	−28 57 14.9	1.7×0.0, 78	1.5	2.2		5	−0.8	−0.5 (L)	−0.26 (GC)	FR-II
	C	17 44 36.84	−28 57 11.5	0.2×0.0, 11	7.9	8.1			−0.8	−0.4 (L)		
	W	17 44 37.08	−28 57 09.7		41	46	34		−1.3	−1.0 (L)		
0.404+1.061	E	17 42 27.93	−28 02 08.5	0.4×0.1, 130	13.5	14.8		11	−1.3	−1.0†(i)	−0.9 (GC)	EG-D
	W	17 42 28.25	−28 02 10.9	0.7×0.1, 97	07.5	10.0			−1.3			
1.826+1.070	N	17 45 47.67	−26 49 05.6	1.8×1.3, 176	7.5	20.2		8	−1.3	−0.86	−0.9 (i)	FR-II
	S	17 45 47.17	−26 49 21.5	0.9×0.0, 08	9.8	16.4		23	−1.0	−0.6		
2.922+1.028	N	17 48 29.18	−25 54 15.8	1.1×0.9, 37	13.8	16.7		6	−1.1 s	−0.8 (i)	−0.94	EG-D
	S	17 48 29.09	−25 54 18.0	0.6×0.5, 11	21.3	25.4		8	−1.1 s			
3.347−0.327	C	17 54 38.31	−26 13 50.9	1.7×0.9, 168	4.8	10.3	6	20	−1.2	−1.1†	−1.2 (GM)	EG-SR
3.745+0.635 (1748−253)	C	17 51 51.26	−25 24 0.0	0.0×0.0, 0	446	446		2.6	−1.0	−1.0	0.1 (GM1)	EG-U
3.748−1.221	E	17 58 58.66	−26 20 02.1	0.4×0.0, 27	11.3	12.9		10	−1.3	−1.0†(N) (i)	−0.77 (GM)	EG-D
	W	17 58 59.75	−26 19 56.8	0.0,0.0, 00	2.8	3.1			0.1			
3.928+0.253	C	17 53 43.37	−25 26 10.3	0.2×0.0, 178	120	122	67.9	2	0.2	**	0.0 (GM1)	EG-U
											(0.3/4.8)	
4.752+0.255	C	17 55 33.41	−24 43 30.6	1.2×1.1, 143	26	46	33.2	7	−1.3	−1.1†	−0.8	EG-SR
5.791+0.794	E	17 55 48.31	−23 33 21.9	3.1×1.3, 77	17.7	64		17	−1.4 s	−1.0†(N)	−0.8	EG-T
	C	17 55 48.60	−23 33 21.1	1.9×0.0, 77	10.8	13.9		17	−1.0 s			
	W	17 55 48.82	−23 33 20.5	1.6×1.5, 68	12.7	49		30	−1.3 s			
5.852+1.041	N	17 55 00.75	−23 22 32.4	1.5×0.4, 01	9.2	21.8		12	−1.0	−0.9	−1.1 (i)	EG-D
	S	17 55 00.80	−23 22 52.0	3.4×1.2, 119	2.8	12.8		24	−1.5	−0.75		

Table 4: Measured parameters of the unpolarised sources from the ATCA data

Source	Cmp	RA (J2000)	DEC (J2000)	$Smaj \times S_{min}$, PA	S_p	S_t	S_5	$\alpha_{8.5/4.8}$	$\alpha_{4.8/1.4}$	$\alpha_{1.4/0.3}$	Notes
354.719-1.117	N	17 36 57.84	−34 00 30.0	0.4×0.0, 01	92	91		−0.8	−0.8	−0.6 (i)	EG-D

Source	Cmp	RA (J2000)	DEC (J2000)	$S_{maj} \times S_{min}$, PA	S_p	S_t	S_5	$\alpha_{8.5/4.8}$	$\alpha_{4.8/1.4}$	$\alpha_{1.4/0.3}$	Notes
357.435-0.519	S	17 36 57.19	-34 00 37.6	1.2×0.0, 01	06	07		-1.2	-1.1		EG–SR
358.982+0.580	C	17 41 26.32	-31 23 30.3	6.0×2.0, 167	49	73		-	-0.8	-0.6 (GM)	EG–U
	C	17 40 54.52	-29 29 50.6	0.3×0.0, 7	44	44		-	-0.6†	-0.5 (GC)	EG–U
359.568+1.146	C	17 40 07.79	-28 42 03.0	0.4×0.4, 38	113	114		-	-0.5	-0.4 (GC)	EG–U
358.591+0.046	C	17 42 02.71	-30 06 41.7	1.0×0.0, 26	25	25	17	-0.8	-1.0†	-1.1 (GC)	EG–U
359.546+0.988	C	17 40 41.56	-28 48 10.7	0.0×0.0, 0	35	35		-0.8	-0.8†	-0.5 (GC)	EG–U
0.846+1.173	C	17 43 05.43	-27 36 05.2	1.3×0.0, 7	43	46		-0.9	-1.0	-0.8 (GC)	EG–U
1.954-1.702	C	17 56 49.65	-28 07 37.4	0.7×0.0, 171	60	60		-1.6	-1.1†	-0.4	EG–U
2.423-1.660	C	17 57 43.61	-27 42 02.0	0.6×0.3, 11	46	46		-1.1	-0.8	-1.0	EG–U
4.898+1.292	C	17 51 57.26	-24 04 24.9	0.9×0.0, 26	51	52		-1.3	-1.1	-0.9	EG–U

Table 5: Estimated parameters of the unpolarised sources from the VLA data

Source	Cmp	RA (J2000)	DEC (J2000)	$S_{maj} \times S_{min}$, PA	S_p	S_t	S_5	$\alpha_{8.5/4.8}$	$\alpha_{4.8/1.4}$	$\alpha_{1.4/0.3}$	Notes
353.410-0.360	C	17 30 26.14	-34 41 44.9	2.6×2.1, 51	149	469	155	0.0	0.1		G–HII
355.739+0.131	EX	17 34 34.24	-32 28 34.3	~12×10, -	28	256	155	-0.1	0.1		G–HII
358.643-0.034	EX	17 42 29.08	-30 06 34.6	~20×20, -	07	169	48	-1.2	0.4		G–HII
358.605+1.440	C	17 36 38.76	-29 21 26.4	0.4×0.0, 17	39	40		-0.8	-0.7	-0.7	EG–U
359.717-0.036	R	17 45 05.08	-29 11 45.0	~22×20, -	12	198[1]	28	-1.3	-		G–HII
4.005+0	C	17 54 38.87	-25 27 30.7	1.0×0.0, 165	08	09[2]		-0.8	-0.8	-	EG–M
4.619+0.288	C	17 55 07.96	-24 49 21.7	0.8×0.3, 10	22	25	21	-1.1	-0.9†	-0.45	EG–SR

[1] flux density of the component near the bottom of its map (Fig. 6)
[2] flux density of the component near the top of its map (Fig. 6)
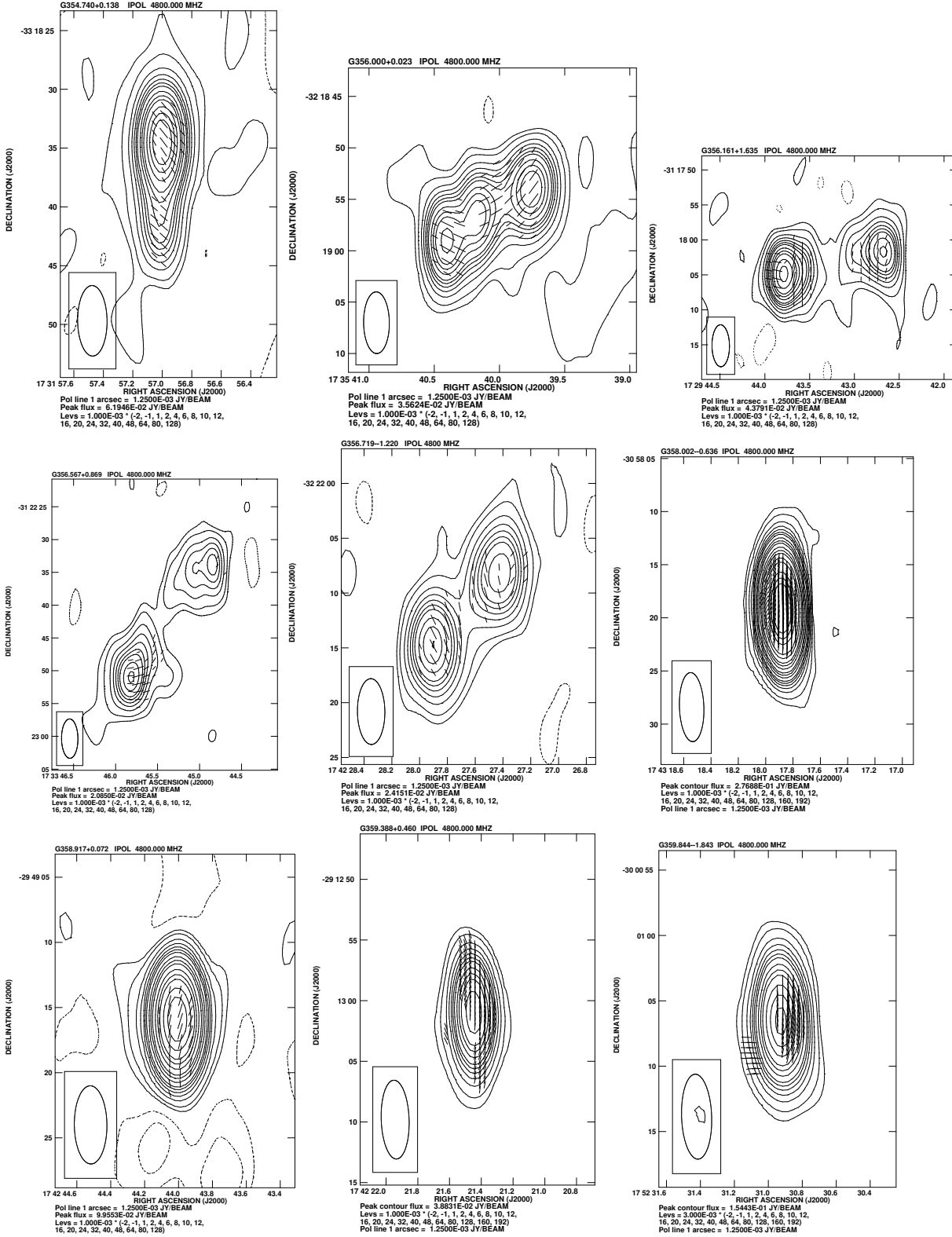
Figure 3. 4.8 GHz ATCA continuum images of the polarised sources with the polarisation vectors representing the projected electric field superposed on them. Typical rms noise in Stokes I is about 0.23 mJy/beam and about 0.15 mJy/beam in Stokes Q and U. Typical beamsize of these images are $\approx 6'' \times 2''$.
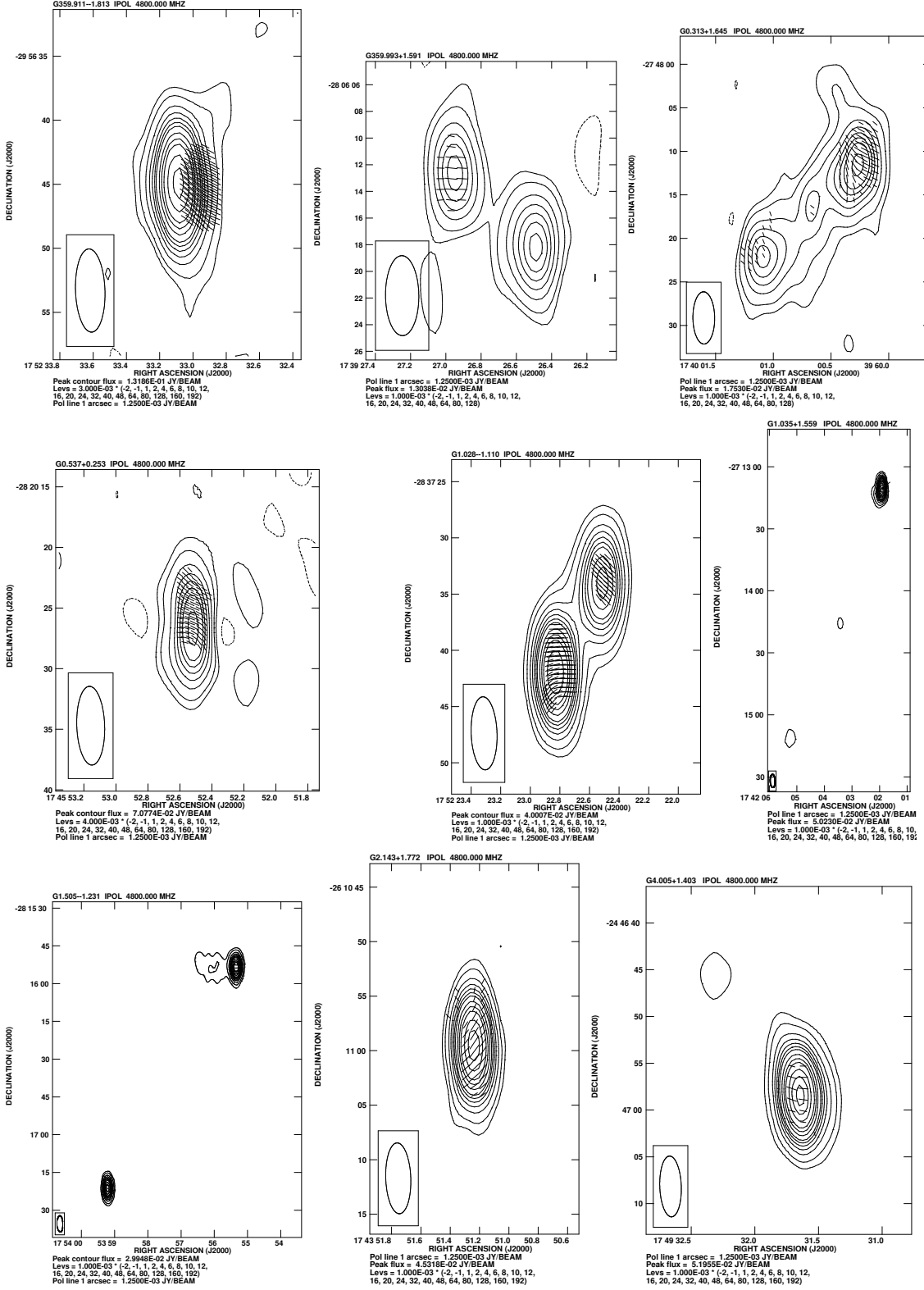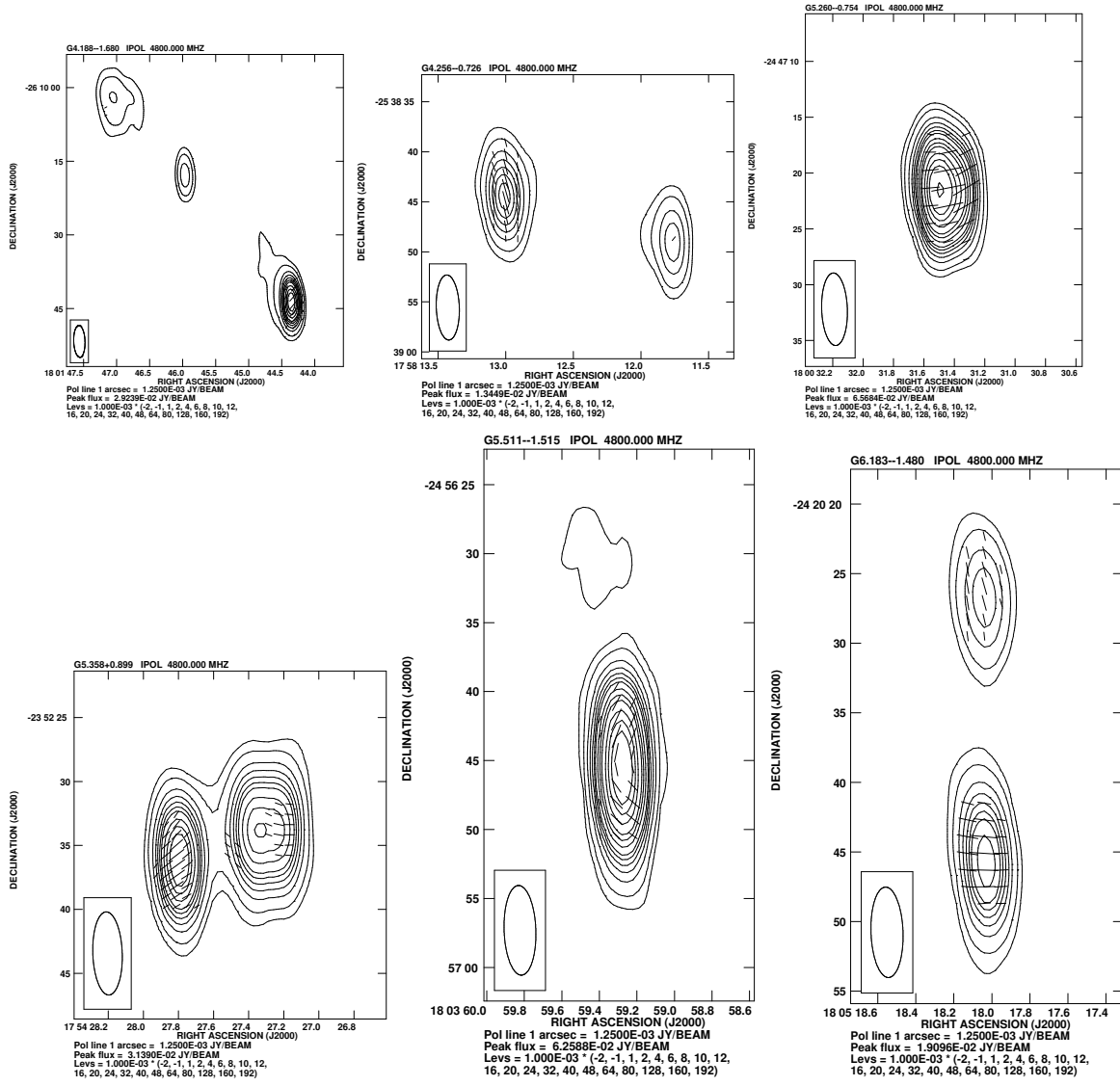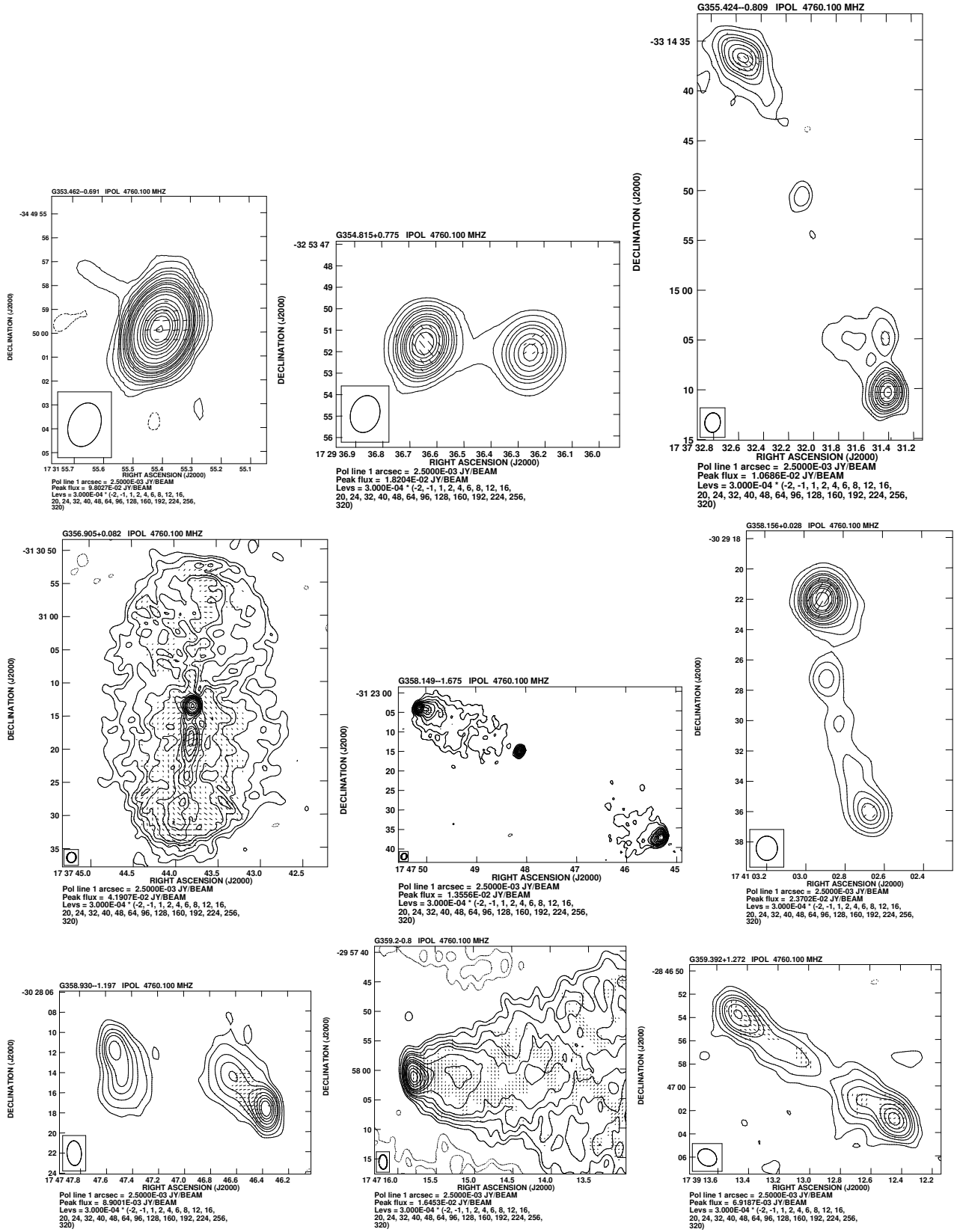
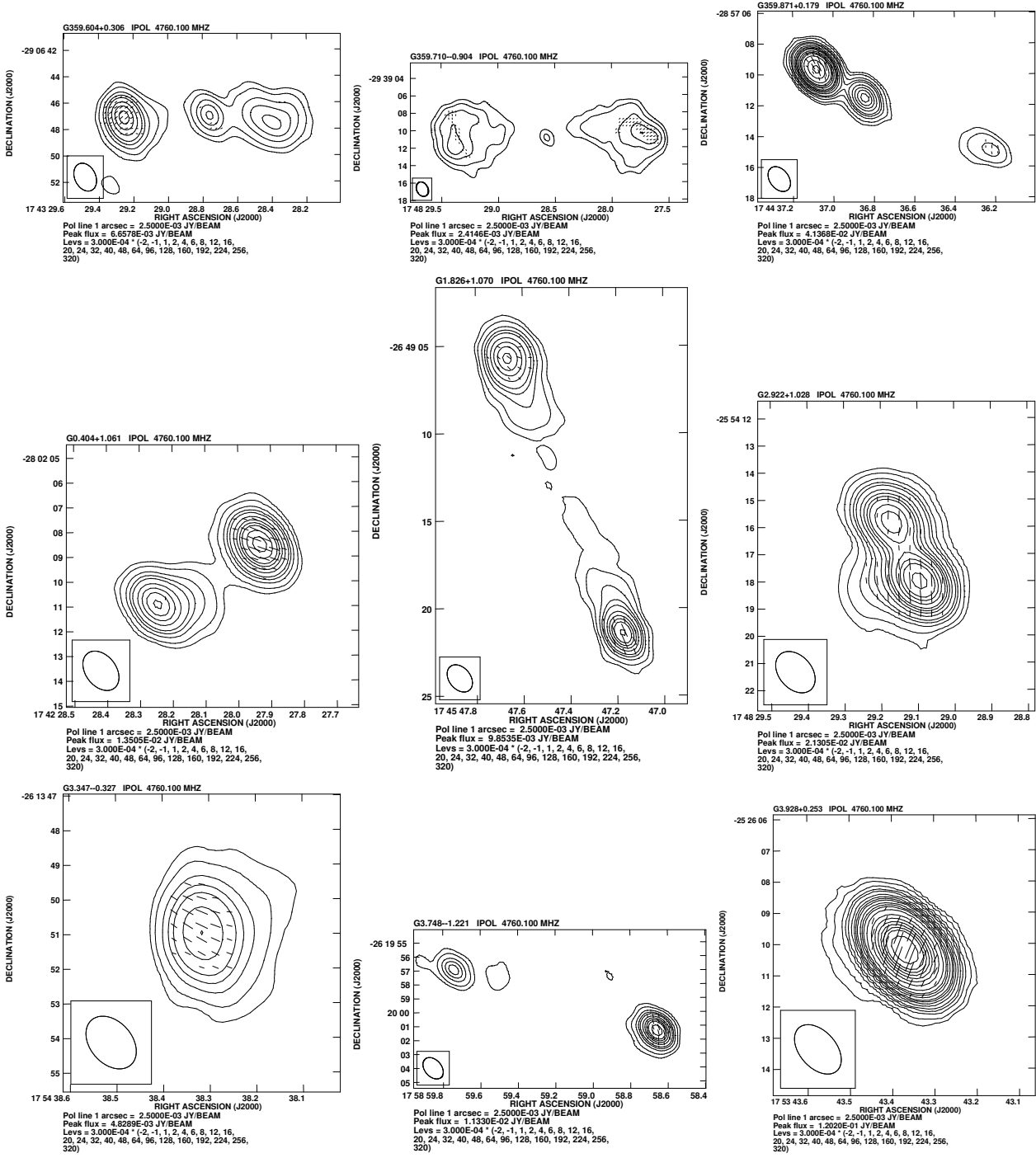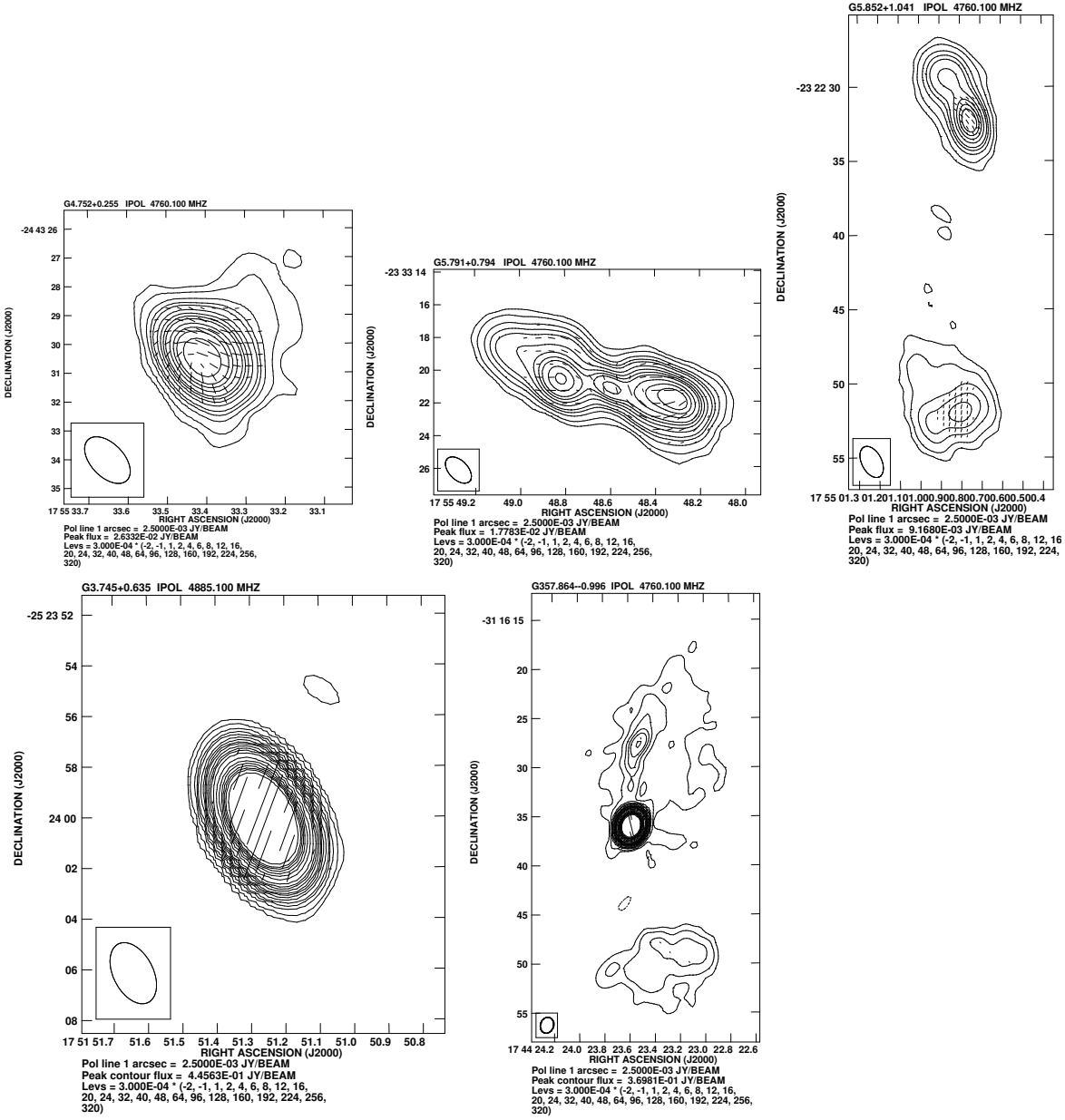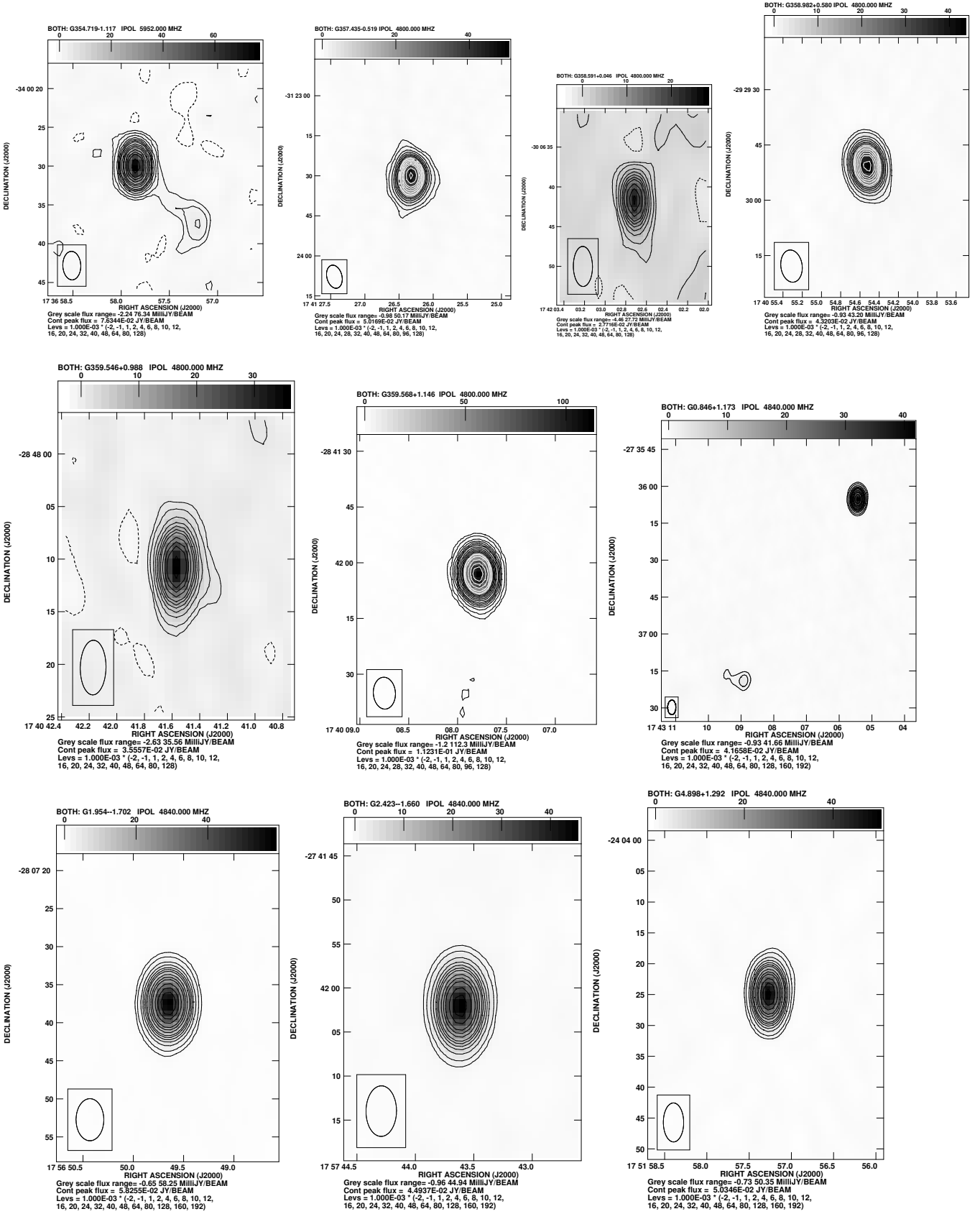**Figure 3.** Continued

Figure 3. Continued

Figure 4. 4.8 GHz VLA continuum maps of the polarised sources with the polarisation vectors superposed on them. Typical rms noise in Stokes I is about 90 μJy/beam and about 75 μJy/beam in Stokes Q and U. Typical beamsize of these images are $\approx 2'' \times 1.5''$.

Figure 4. Continued

Figure 4. Continued

Figure 5. 4.8 GHz continuum images of the unpolarised sources observed with the ATCA. Typical rms noise in Stokes I is about 0.23 mJy/beam, and beamsize ≈6″ × 2″.
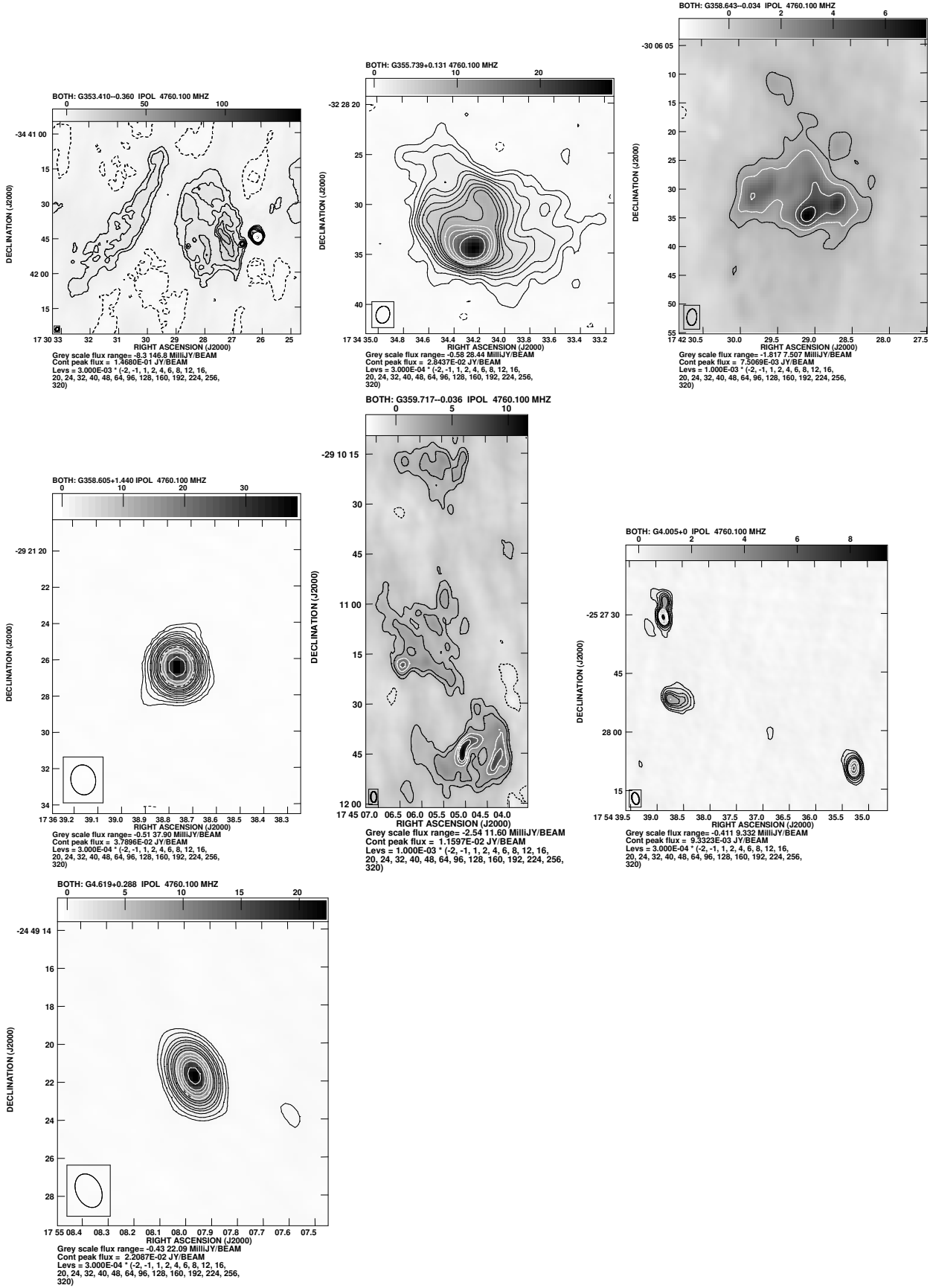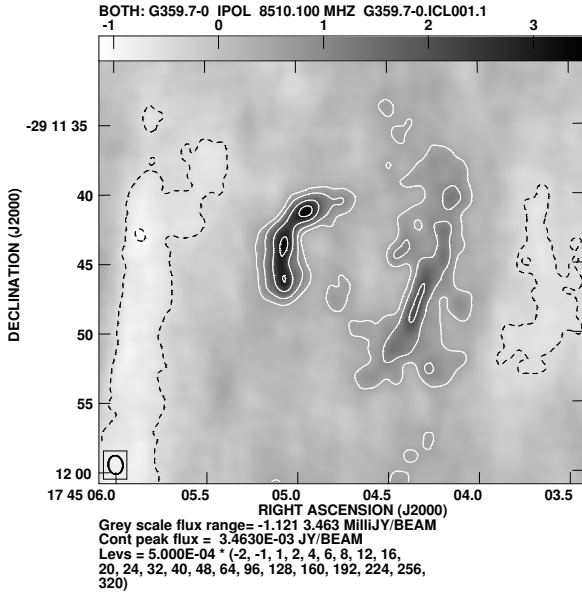
Figure 6. 4.8 GHz continuum image of the unpolarised sources observed with the VLA. Typical rms noise is about 90 μJy/beam, and beamsize of $\approx 2'' \times 1.5''$.

Table 6: Estimated RM towards the background sources towards the GC region

Source Name	RA (J2000)	DEC (J2000)	RM	Error on RM	D	Δ(D) (%)	θ	Δθ	χ²	Measured polarisation angles at different frequencies
353.462-0.691	17 31 55.40	-34 49 59.9	1011	30	0.5	14	123	5.7	2.3	8540 -83±5.4, 8484 -67±5.5, 4885 74±4.8, 4635 94± 3.7
354.740+0.138	17 31 56.96	-33 18 33.72	1193	32	0.7	15	49	5.8	4.6	8512 39±4.1, 5952 -46±3.8, 5312 04 ±3.1, 4804 41±2.9
	17 31 57.00	-33 18 42.12	858	45	0.8	25	122	8.1	2.7	8512 -85±6.2, 5952 -33±4.6, 5312 07 ±3.8, 4804 44±4.8, 4764 52±5.7
354.815+0.775	17 29 36.653	-32 53 51.88	-99	16	0.8	10	153	2.7	0.1	8685 57±2.6, 8335 55±2.4, 4885 42±2.6, 4635 39±2.5
355.424-0.809	17 37 32.514	-33 14 36.88	611	17	0.9	11	167	3.5	4.0	8685 -58±3.1, 8335 -60±3.9, 4885 25±2.1, 4635 47±1.9
	17 37 31.413	-33 15 09.56	574	23	0.9	17	37	4.6	1.1	8685 -20±5.4, 8335 -07±3.8, 4885 70±2.8, 4635 85±2.4
356.000+0.023	17 35 40.37	-32 18 59.03	328	25	1.1	15	79	4.6	0.5	8512 11±4.0, 5952 39±2.0, 5312 49±1.8, 4804 63±1.8
	17 35 40.05	-32 18 55.83	439	29	0.9	15	112	5.1	3.0	8512 54±4.0, 5952 83±2.3, 5312 -73±2.5, 4804 -62±2.5
	17 35 39.74	-32 18 54.23	720	30	1.1	17	73	5.6	0.2	8512 33±4.8, 5952 89±2.6, 5312 -66±2.3, 4804 -36±2.3
356.161+1.635	17 29 43.86	-31 18 04.77	679	27	1.0	16	13	4.9	3.9	8512 39±4.1, 5952 -46±3.8, 5312 04±3.1, 4804 41±2.9
	17 29 43.64	-31 18 04.77	681	23	1.4	20	109	4.4	2.5	8512 61±4.7, 5952 -58±1.8, 5312 -36±1.6, 4804 -08±1.4
	17 29 42.71	-31 18 02.37	629	34	0.9	18	119	6.4	3.8	8512 68±5.0, 5952 -58±3.9, 5312 -29±3.4, 4804 -14±2.6
356.567+0.869	17 33 45.73	-31 22 50.38	960	35	1.1	12	163	6.5	0.2	8512 -37±3.7, 5952 31±2.4, 5312 70±2.1, 4804 -72±1.8
356.719-1.220	17 42 27.90	-32 22 14.04	-511	37	1.1	23	51	6.7	1.8	8512 -83±6.6, 5952 70±2.5, 5312 46±2.4, 4804 27±2.6
	17 42 27.52	-32 22 09.64	-464	41	1.2	23	27	7.6	3.3	8512 82±6.7, 5952 56±3.6, 5312 27±3.2, 4804 16±2.8
357.865-0.996 (1741-312)	17 44 23.580	-31 16 35.970	1883	2.9	0.8	1.3	151	0.4	5.5	8512 14.7±0.3, 5952 -24.3±0.3, 5312 45.8±0.3, 4804 -59.3±0.4
358.002-0.636	17 43 17.87	-30 58 18.73	869	13	1.4	09	76	2.0	17	8685 50±1.7, 8335 51±2.2, 5988 -79±2.6, 5920 -83±2.6, 4836 -01±2.5, 4764 06±1.9
358.149-1.675	17 47 50.144	-31 23 03.86	-22	13	0.9	09	142	2.6	4.0	8685 46±2.5, 8335 56±2.5, 4885 48±1.7, 4635 47±1.6
	17 47 45.300	-31 23 36.21	276	18	1.0	12	156	3.6	0.4	8685 85±3.7, 8335 88±3.3, 4885 -55±1.9, 4635 -46±1.9
	17 47 45.411	-31 23 38.40	346	24	1.4	18	102	5.1	0.3	8685 34±4.9, 8335 41±5, 4885 87±2.1, 4635 -84±2.1
358.156+0.028	17 41 02.909	-30 29 22.11	533	7	0.9	05	112	1.3	2.4	8685 57±1.3, 8335 62±1.2, 4885 -42±0.8, 4635 -31±0.8
	17 41 02.668	-30 29 36.53	469	28	1.1	17	117	5.1	0.5	8685 58±4.8, 8335 62±5.3, 4885 -50±3.1, 4635 -44±4.5
358.917+0.072	17 42 43.99	-29 49 16.03	4768	88	0.3	10	95	3.9	1.3	8512 -17±2.3, 5988 -37±3.3, 5952 -26±3.3, 5920 -20±4.1, 5312 -3.6±3.9, 4804 -12±4.7
358.930-1.197	17 47 46.474	-30 28 17.39	-905	26	1.0	17	71	4.9	9.4	8685 -69±4.4, 8335 77±5.1, 4885 -31±4.4, 4635 -57±3.1
359.2-0.8 (Mouse)	17 47 15.78	-29 58 01.0	-05	18	1.0	06	94	3.4	1.0	8685 -7±2.9, 8335 -2±4.0, 4885 -8.2±2.3, 4635 -5±2.4
359.388+0.460	17 42 21.47	-29 12 59.73	-568	29	0.4	10	36	4.2	0.9	8512 85±2.7, 5988 54±4, 5920 42±4.0, 5660 36.6±5.6, 5312 24±4.1, 4804 -1.5±4.5

Source Name	RA (J2000)	DEC (J2000)	RM	Error on RM	D	ΔD (%)	θ	Δθ	χ²	Measured polarisation angles at different frequencies
359.392+1.272	17 39 13.384	−28 46 54.08	−318	27	1.2	20	53	5.4	1.7	8685 −55±5.4, 8335 −63±5.0, 4885 70±3.3, 4635 70±3.3
	17 39 12.505	−28 47 01.35	−271	30	1.1	20	66	5.5	0.2	8685 −40±5.3, 8335 −46±5.3, 4885 −83±3.8, 4635 −88±4.4
359.604+0.306	17 43 29.266	−29 06 46.736	−502	34	–	–	162	7.2	0.3	8685 38±5.0, 5056 −32±4.7, 4885 −35±5.2, 4635 −48±3.0
359.710-0.904	17 48 29.373	−29 39 08.83	1423	93	–	–	117	19	2.2	5696 79±6.1, 5056 −50±4.1, 4885 −31±5.0, 4635 14±4.7
	17 48 27.686	−29 39 09.76	1475	52	–	–	28	11	1.8	5696 −07±3.0, 5056 57±3.1, 4885 72±2.9, 4635 −65±3.3
359.844-1.843	17 52 30.88	−30 01 06.59	−58	47	–	–	96	9.4	0.3	5988 −03±3.8, 5920 00±4.4, 4836 −7.7±3.4, 4764 −6±3.4
359.871+0.179	17 44 37.069	−28 57 09.27	772	14	0.9	10	106	2.7	0.2	8685 68±2.8, 8335 75±2.7, 4885 03±1.4, 4635 22±1.5
359.911-1.813	17 52 32.97	−29 56 44.28	165	47	–	–	116	9.0	0.3	5952 49±4.6, 5696 52±2.7, 5056 61±2.8, 4804 62±2.3
359.993+1.591	17 39 26.94	−28 06 12.65	16	41	0.7	20	172	7.4	1.3	8512 80±5.3, 5952 −89±5.4, 5312 89±5.3, 4804 84±3.5
0.313+1.645	17 40 0.21	−27 48 10.37	−121	22	1.1	12	00	4.0	0.5	8512 82±3.2, 5952 74±2.2, 5312 67±1.7, 4804 64±1.7
0.404+1.061	17 42 27.934	−28 02 08.49	−176	16	0.8	12	21	3.2	0.4	8685 −82±3.8, 8335 −82±2.8, 4885 71±1.9, 4635 69±1.7
0.537+0.263	17 45 52.50	−28 20 26.64	−1176	26	0.7	15	56	3.5	2.7	8512 63±1.9, 5952 −30±3.1, 5344 −59±3.8, 5284 −60±5.6, 4836 62±6.7, 4764 48±6.0
1.028-1.110	17 52 22.81	−28 37 41.31	−65	23	0.7	12	22	4.0	0.7	8512 −75±3.1, 5952 −76±2.2, 5312 −80±2.0, 4804 −84±2.0
	17 52 22.51	−28 37 32.51	218	43	0.7	20	83	7.5	0.7	8512 10±6.0, 5952 25±3.4, 5312 29±3.7, 4804 44±3.8
1.035+1.559	17 42 1.90	−27 13 9.94	−136	9	–	–	67	1.6	0.4	5988 −41.7±0.8, 5920 −43.2±0.8, 4836 −52.6±0.7, 4764 −53.6±0.7
1.505-1.231	17 53 55.37	−28 15 53.77	385	12	1.0	07	95	2.2	1.6	8512 33±1.9, 5952 62±1.0, 5312 74±1.1, 4804 −88±0.9
	17 53 59.21	−28 17 21.35	689	24	1.4	15	00	5.0	1.3	8512 −36±4.1, 5952 09±1.8, 5312 37±1.8, 4804 65±1.6
1.826+1.070	17 45 47.185	−26 49 21.48	806	9.5	1.1	07	100	2.0	1.3	8685 64±1.8, 8335 72±2.8, 4885 3.6±1.1, 4635 24.5±1.1
	17 45 47.702	−26 49 06.24	638	40	0.6	23	152	6.9	3.9	8685 −63±6.4, 8335 −83±6.3, 4885 14±7.0, 4635 38±6.2
2.143+1.772	17 43 51.24	−26 10 59.24	158	50	–	–	18	9.8	0.01	5952 −49±3.8, 5696 −47±3.4, 5056 −40±2.5, 4804 −37±2.8
2.922+1.028	17 48 29.121	−25 54 17.97	1563	15	1.0	11	78	3.1	0.3	8685 −83±3.0, 8335 −77±2.9, 4885 −34±1.6, 4635 04±1.6
	17 48 29.150	−25 54 15.97	1510	21	0.7	13	85	3.8	1.4	8685 −79±4.5, 8335 −75±3.1, 4885 −35±3.4, 4635 −05±2.9
3.347-0.327	17 54 38.331	−26 13 50.76	−68	21	0.8	15	166	4.1	0.3	8685 71±3.2, 8335 74±5.5, 4885 60±3.2, 4635 61±2.7
3.745+0.635 (1748-253)	17 51 51.26	−25 24 0.05	1295	2	0.7		115.3	0.4	3.8	8512 −62.1±0.3, 5952 33.4±0.2, 5312 81.8±0.2, 4804 −45.1±0.2
3.748-1.221	17 58 58.649	−26 20 01.31	1247	18	0.8	12	167	3.5	0.9	8685 −17±3.4, 8335 −11±3.6, 4885 −16±2.1, 4635 18±2.2
3.928+0.253	17 53 43.371	−25 26 10.26	1457	7	1.4	04	80	1.2	3.7	8685 88±1.1, 8335 −80±1.2, 4885 −54±1.0, 4635 −21±1.0

Source Name	RA (J2000)	DEC (J2000)	RM	Error on RM	D	Δ(D) (%)	θ	Δθ	χ²	Measured polarisation angles at different frequencies
4.005+1.403	17 49 31.68	−24 46 57.70	490	28	0.8	10	68	5.0	3.4	8512 06±3.8, 5952 54±2.5, 5312 70±2.8, 5284 69±4.8, 4836 75±5.3, 4764 83±4.3
4.188-1.680	18 01 44.34	−26 10 43.63	−625	15	1.0	08	12	2.8	1.0	8512 55±2.3, 5952 11.5±1.4, 5312 −12±1.3, 4804 −39±1.1
4.256-0.726	17 58 12.97	−25 38 44.29	1788	22	0.7	12	73	3.9	3.6	8512 −74±3.2, 5952 64±1.8, 5312 −46±2.4, 4804 20±1.7
4.752+0.255	17 55 33.409	−24 43 29.77	191	18	0.9	13	110	3.7	3.2	8685 27±3.6, 8335 40±3.5, 4885 63±2.1, 4635 65±1.9
	17 55 33.424	−24 43 31.16	112	24	0.7	17	65	4.8	0.2	8685 −19±5.3, 8335 −16±4.1, 4885 01±3.7, 4635 01±2.6
5.260-0.754	18 00 31.38	−24 47 21.73	1145	12	0.7	06	126	2.1	0.7	8512 −62±1.6, 5952 22±1.3, 5312 64±1.3, 4804 −67.5±1.1
5.358+0.899	17 54 27.81	−23 52 36.17	851	29	0.8	15	29	5.3	2.0	8512 −04±4.2, 5952 68±2.8, 5312 −86±2.2, 4804 −51±2.4
5.511-1.515	18 3 59.28	−24 56 43.63	319	20	0.8	09	01	3.5	0.5	8512 −65±2.6, 5952 −44±1.9, 5312 −31±2.1, 4804 −17±2.0
	18 3 59.25	−24 56 48.03	396	32	1.2	17	50	6.1	1.4	8512 −13±4.6, 5952 23±4.4, 5312 29±3.0, 4804 49±2.3
5.791+0.794	17 55 48.323	−23 33 22.71	1203	13	0.9	11	91	2.8	2.8	8685 79±2.8, 8335 −85±2.7, 4885 82±1.3, 4635 −70±1.2
	17 55 48.526	−23 33 21.09	1294	17	1.1	13	155	3.5	0.2	8685 −25±3.1, 8335 −21±4.3, 4885 −15±1.8, 4635 16±1.7
	17 55 48.802	−23 33 18.67	1144	24	1.4	17	66	4.9	0.8	8685 55±5.6, 8335 59±4.4, 4885 45±2.1, 4635 69±2.1
5.852+1.041	17 55 00.749	−23 22 31.56	581	26	1.0	18	172	5.3	2.7	8685 −58±4.5, 8335 −52±6.3, 4885 22±3.0, 4635 45±2.6
	17 55 00.800	−23 22 52.16	623	33	0.8	23	113	6.7	0.1	8685 66±6.2, 8335 69±6.9, 4885 −21±3.6, 4635 −08±3.6
6.183-1.480	18 5 18.04	−24 20 45.50	−876	24	0.9	12	10	4.4	3.8	8512 44±3.5, 8952 −27±2.0, 5348 −63±2.4, 5312 −64±1.7, 5284 −66±3.1, 4764 −95±2.3

BOTH: G359.7-0 IPOL 8510.100 MHZ G359.7-0.ICL001.1

Figure 7. 8.5 GHz continuum image of the object G359.717−0.036 with a partial shell morphology

4 DISCUSSION

4.1 Galactic HII regions

Extended unpolarised structures, typical of HII regions, are seen in the VLA images of the sources G353.410−0.360, G355.739+0.131, G358.643−0.034 and G359.717−0.036. A small diameter source is seen in the field of G353.410−0.360, which has a flat spectrum between 8.5 and 4.8 GHz. It is well resolved in our BnA array image and is unlikely to be the flat spectrum core of a background extragalactic source. We believe that it is a Galactic HII region.

The 8.5 GHz VLA BnA array image of G359.717−0.036 (Fig. 7) shows a partial shell-like structure. Extended emission can also be seen around this object. Since either HII regions or shell type SNRs can have shell like morphology, we have tried to measure its spectral index accurately. We made an image of this object at 8.4 GHz using the archival VLA CD array data (Project Code AY68 made by Farhad Yusef Zadeh). We also imaged it at 1.4 GHz using the archival Galactic Centre data acquired and presented by Pedlar et al. (1989) using the B, C and D array of the VLA during 1981–1984. From the low resolution 8.4 and 1.4 GHz image of this source, the measured spectrum of this component is flat, indicating it to be an HII region.

The image of G358.643−0.034 at 8.5 GHz suffers from missing short spacings and, consequently, the measured steep spectral index between 8.5 and 4.8 GHz (Table 5) is underestimated. However, its spectrum between 4.8 and 1.4 GHz is inverted and the source is not detected in the 330 MHz GC image. The extended structure and inverted spectrum at low frequencies suggest that it is an HII region.

G355.739+0.131 has a flat spectrum between 8.5 and 1.4 GHz and is well resolved. This source is also not detected at 0.3 GHz, which suggests that its spectrum has turned over due to significant free-free absorption at low radio frequencies: these suggest that the source is an HII region.

4.2 Are the rest of the sources extragalactic ?

Excluding the sources described above, the rest of the sources observed are either polarised or the deconvolved diameters imply a brightness temperature greater than 10^3 K at 4.8 GHz. Except for a few small diameter sources, all the other sources have steep spectral indices indicating the emission from these sources is non-thermal. The small diameter objects have flat spectra ($\alpha \geqslant -0.3$) down to 0.3 GHz. A thermal source with brightness temperature of 10^3 K at 4.8 GHz should show self absorption (i.e., positive spectral index) at 0.3 GHz (otherwise, the required brightness temperature exceeds 10^5 K). Therefore, these objects with flat spectra at 0.3 GHz indicate that the emission from these small diameter sources are also non-thermal. Among the non-thermal sources, the object G359.2−0.8 (Mouse) (Table 3) (Yusef-Zadeh & Bally 1987; Uchida et al. 1992) is known to be a Galactic non-thermal source located within 5 kpc from the Sun. We review below non-thermal emission from Galactic objects with the aim of rejecting any of the remaining sources in the sample, which might admit such a classification.

4.2.1 *Non thermal emission from Galactic sources*

There are several types of Galactic sources that emit non-thermal emission.

(i) Supernova Remnants (SNRs): These are the remnants of supernova explosions. The electrons in these objects are accelerated to high energies near the expanding shock front. The SNRs are usually spherical in shape, and when projected on the sky appear like a ring for the shell type SNRs, while they appear to be filled with emission in the case of plerion-type SNRs. None of the non-thermal objects in Tables 2, 3, 4 & 5 have such a morphology, indicating that there is no resolved supernova remnant among these sources. However, if an SNR is young, its angular size will be small and will appear like an unresolved source. Assuming an initial expansion velocity of 3000 km s^{-1}, an SNR at a distance of 10 kpc will expand to an angular size of $6''$ in about 100 years after the explosion. An object of angular size of $6''$ will be well resolved in our images and should have a ring or filled centre morphology: the absence of these rule out any SNR older than 100 years in our sample. Since the expected number of supernova explosions in our Galaxy is believed to be about 1 in 50 years, the probability of finding an SNR of age less than 100 years in the central $12° \times 4°$ of the Galaxy is less than 0.1, which suggests that there is no young SNR in our sample.

(ii) Radio Pulsars: Pulsars typically have a very steep spectrum, with spectral indices of −1.5 to −4 at cm wavelengths. They would be unresolved and almost all would be undetectable at 5 GHz owing to their steep spectrum. Since none of the unresolved sources in our sample have a very steep spectrum, we believe that there is no pulsar in our list of sources.

(iii) Radio Stars: Most stars are weak radio emitters; however, some are detected in non-thermal emission. Becker et al. (1994) show that the radio flux densities from these stars are ⩽1 mJy at 5 GHz. Since the observed flux densities of our sources are much higher than the upper limit for these stars, such objects can be ruled out from our list of sources.

(iv) Transient sources: These are highly variable and transient radio sources which include radio counterparts of X-ray sources. The sources in our sample are not only detected at 4.8 and 8.5 GHz, but also detected at 1.4 GHz in the GPS and the NVSS. These sources are also detected at 0.3 GHz, either in the Texas survey or in the 330 MHz GC observations. These observations were separated

by days to years and the measured spectral indices determined between any two bands are quite close to the mean value (differences are less than 0.6). Therefore, the flux densities of these sources have not changed by more than a factor of two and this rules out the possibility that there are transient sources in our catalogue.

(iv) Galactic Microquasar: These are stellar-mass black holes in our Galaxy that mimic, on a smaller scale, many of the phenomena seen in quasars (see Mirabel & Rodríguez (1999), and the references therein). For a black hole accreting at the Eddington limit, the characteristic black body temperature at the last stable orbit in the surrounding accretion disk is given by $T \sim 2 \times 10^7 M^{-1/4}$ (Rees 1984). Therefore, compared to the AGNs, the emission from microquasars are shifted towards higher frequencies and the microquasars are usually identified by their X-ray properties (Mirabel & Rodríguez 1999).

Though many of the already known microquasars are highly variable, two of these sources, 1E1740.7−2942 (Mirabel & Rodríguez 1999) and GRS 1758−258 (Martí et al. 2002), are persistent sources of both X-rays and relativistic jets. At radio wavelengths, these two sources are morphologically similar to typical radio galaxies, which have a central compact component and two extended lobes. Therefore, based on morphology, microquasars cannot be separated from the distant radio galaxies. However, as mentioned above, microquasars are believed to have X-ray counterparts. We have searched the ROSAT PSPC all sky survey (Voges et al. 1999) and a catalogue of soft X-ray sources ($|l| \leqslant 1.5°$, $|b| \leqslant 2.0°$) in the GC region (Sidoli et al. 2001). Twenty of our sources are also located within the boundary of the ASCA survey of the GC region ($|l| \leqslant 2.5°$, $|b| \leqslant 2.5°$) (Sakano et al. 2002). However, none of the radio sources in our sample were found to have any counterpart in these catalogues. Therefore, it is unlikely that any of the sources we have observed (Tables 2, 3, 4 & 5) is a microquasar.

4.3 Extragalactic source counts

The expected number of extragalactic sources (N) in 1 square arc minute of the sky at 5 GHz and with a flux density limit of S mJy is $N(>S)= 0.032 \times S^{-1.13}$ (Ledden et al. 1980). Therefore, the expected number of extragalactic sources seen through the central $l \times b = 12° \times 3.6°$ region of the Galaxy above a flux density limit of 20 mJy at 5 GHz is 168. However, as we selected sources with steep spectral indices ($\alpha < -0.4$), typical sizes $\leqslant 10''$ and excessive confusion prevails in the region, we could identify only 59 extragalactic sources, which indicates that about two thirds of the extragalactic sources in this region are yet to be identified. The median angular size of these 59 sources is $7.6''$, and the median flux density at 1.4 GHz is 160 mJy.

5 SUMMARY

We have observed 64 sources towards the central $-6° < l < 6°$, $-2° < b < 2°$ of the Galaxy using the 6 and 3.6 cm band of the ATCA and the VLA. Based on our work described herein, 59 of these sources are classified to be extragalactic. This increases the number of known extragalactic radio sources towards this unique region by almost an order of magnitude and provides the first systematic study of the polarisation properties of the background sources in the region. We provide 4.8 GHz images of all the observed sources and measure the angular sizes and the spectral indices of these sources. Based on the morphology, spectral char-

acteristics and polarisation properties, we identify 4 Galactic HII regions in the sample.

REFERENCES

Becker R. H., White R. L., Helfand D. J., Zoonematkermani S., 1994, ApJS, 91, 347
Bevington P. 1969, Data Reduction and Error Analysis for the Physical Sciences (New York: McGraw-Hill)
Bower G. C., Backer D. C., Sramek R. A., 2001, ApJ, 558, 127
Condon J. J., Cotton W. D., Greisen E. W., Yin Q. F., Perley R. A., Taylor G. B., Broderick J. J., 1998, AJ, 115, 1693
Douglas J. N., Bash F. N., Bozyan F. A., Torrence G. W., Wolfe C., 1996, VizieR Online Data Catalog, 8042, 0
Gardner F. F., Whiteoak J. B., 1966, ARA&A, 4, 245
Helfand D. J., Zoonematkermani S., Becker R. H., White R. L., 1992, ApJS, 80, 211
Kronberg P. P., Conway R. G., Gilbert J. A., 1972, MNRAS, 156, 275
LaRosa T. N., Kassim N. E., Lazio T. J. W., Hyman S. D., 2000, AJ, 119, 207
Lazio T. J. W., Anantharamaiah K. R., Goss W. M., Kassim N. E., Cordes J. M., 1999, ApJ, 515, 196
Lazio T. J. W., Cordes J. M., 1998, ApJS, 118, 201
Ledden J. E., Broderick J. J., Brown R. L., Condon J. J., 1980, AJ, 85, 780
Lovell J. E. J., Jauncey D. L., Bignall H. E., Kedziora-Chudczer L., Macquart J.-P., Rickett B. J., Tzioumis A. K., 2003, AJ, 126, 1699
Martí J., Mirabel I. F., Rodríguez L. F., Smith I. A., 2002, A&A, 386, 571
Mirabel I. F., Rodríguez L. F., 1999, ARA&A, 37, 409
Pedlar A., Anantharamaiah K. R., Ekers R. D., Goss W. M., van Gorkom J. H., Schwarz U. J., Zhao J., 1989, ApJ, 342, 769
Roy S., Rao A. P., 2002, MNRAS, 329, 775
Saikia D. J., Salter C. J., 1988, ARA&A, 26, 93
Sakano M., Koyama K., Murakami H., Maeda Y., Yamauchi S., 2002, ApJS, 138, 19
Sidoli L., Belloni T., Mereghetti S., 2001, A&A, 368, 835
Simard-Normandin M., Kronberg P. P., 1980, ApJ, 242, 74
Uchida K., Morris M., Yusef-Zadeh F., 1992, AJ, 104, 1533
Vallee J. P., 1980, A&A, 86, 251
Voges W., Aschenbach B., Boller T., Bräuninger H., Briel U., Burkert W., Dennerl K., Englhauser J., 1999, A&A, 349, 389
Wagner S. J., Witzel A., 1995, ARA&A, 33, 163
Yusef-Zadeh F., Bally J., 1987, Nature, 330, 455
Zoonematkermani S., Helfand D. J., Becker R. H., White R. L., Perley R. A., 1990, ApJS, 74, 181